Reichel *et al. BMC Plant Biology* (2024) 24:552
https://doi.org/10.1186/s12870-024-05249-4

BMC Plant Biology

RESEARCH Open Access

Revealing the Arabidopsis *AtGRP7* mRNA binding proteome by specific enhanced RNA interactome capture

Marlene Reichel[1,2*], Olga Schmidt[1], Mandy Rettel[3], Frank Stein[3], Tino Köster[1], Falk Butter[4] and Dorothee Staiger[1*]

Abstract

Background The interaction of proteins with RNA in the cell is crucial to orchestrate all steps of RNA processing. RNA interactome capture (RIC) techniques have been implemented to catalogue RNA- binding proteins in the cell. In RIC, RNA-protein complexes are stabilized by UV crosslinking in vivo. Polyadenylated RNAs and associated proteins are pulled down from cell lysates using oligo(dT) beads and the RNA-binding proteome is identified by quantitative mass spectrometry. However, insights into the RNA-binding proteome of a single RNA that would yield mechanistic information on how RNA expression patterns are orchestrated, are scarce.

Results Here, we explored RIC in Arabidopsis to identify proteins interacting with a single mRNA, using the circadian clock-regulated *Arabidopsis thaliana GLYCINE-RICH RNA-BINDING PROTEIN 7* (*AtGRP7*) transcript, one of the most abundant transcripts in Arabidopsis, as a showcase. Seedlings were treated with UV light to covalently crosslink RNA and proteins. The *AtGRP7* transcript was captured from cell lysates with antisense oligonucleotides directed against the 5'untranslated region (UTR). The efficiency of RNA capture was greatly improved by using locked nucleic acid (LNA)/DNA oligonucleotides, as done in the enhanced RIC protocol. Furthermore, performing a tandem capture with two rounds of pulldown with the 5'UTR oligonucleotide increased the yield. In total, we identified 356 proteins enriched relative to a pulldown from *atgrp7* mutant plants. These were benchmarked against proteins pulled down from nuclear lysates by *AtGRP7 in vitro* transcripts immobilized on beads. Among the proteins validated by in vitro interaction we found the family of Acetylation Lowers Binding Affinity (ALBA) proteins. Interaction of ALBA4 with the *AtGRP7* RNA was independently validated via individual-nucleotide resolution crosslinking and immunoprecipitation (iCLIP). The expression of the *AtGRP7* transcript in an *alba* loss-of-function mutant was slightly changed compared to wild-type, demonstrating the functional relevance of the interaction.

Conclusion We adapted specific RNA interactome capture with LNA/DNA oligonucleotides for use in plants using *AtGRP7* as a showcase. We anticipate that with further optimization and up scaling the protocol should be applicable for less abundant transcripts.

Keywords Enhanced RNA interactome capture, Arabidopsis, LNA oligonucleotides, iCLIP

*Correspondence:
Marlene Reichel
marlene.reichel@bio.ku.dk
Dorothee Staiger
dorothee.staiger@uni-bielefeld.de
[1]RNA Biology and Molecular Physiology, Faculty of Biology, Bielefeld University, 33615 Bielefeld, Germany
[2]Department of Biology, University of Copenhagen, København N 2200, Denmark
[3]Proteomics Core Facility, EMBL, 69117 Heidelberg, Germany
[4]Institute of Molecular Biology (IMB), Ackermannweg 4, 55128 Mainz, Germany

Background

The interaction of proteins with RNA in the cell is crucial to orchestrate all steps of RNA processing including splicing, nuclear export and decay [1–3]. The identification of RNA-binding proteins (RBPs) interacting with an RNA thus provides insights into RNA biogenesis and function. Research towards assembling a global inventory of proteins binding to RNA in vivo has been enabled by recent technological advancements increasing the sensitivity in mass spectrometry (MS). In RNA Interactome Capture (RIC) approaches, RNA and associated proteins are covalently linked by irradiation with 254 nm UV light. This creates radicals of the nucleobases that react with amino acids in their immediate vicinity. The polyadenylated RNA fraction is then recovered by hybridization with bead-coupled oligo(dT) under stringent conditions. Associated proteins are eluted by ribonuclease digestion and subjected to liquid chromatography/tandem MS, leading to the identification of about 800 mRNA-bound proteins in HeLa and HEK293 cells [4, 5]. Subsequently, RIC was applied to different mammalian cell lines and tissues, and to a range of organisms including yeast [6–8], *Caenorhabditis elegans* [6] or *Drosophila melanogaster* [9, 10], reviewed in [8, 11].

The sensitivity of RIC was increased through the use of locked nucleic acids (LNAs) in the "enhanced RIC" (eRIC) protocol. In LNA nucleosides, a methylene bridge "locks" the ribose between 2'-O and 4'-C, favoring Watson-Crick base-pairing and increasing the stability of duplexes and resistance to nucleases [12]. Furthermore, the oligonucleotides are covalently linked to magnetic beads, thus tolerating more stringent salt conditions and the use of chaotropic detergents employed to reduce non-specific interactions and increase signal-to-noise ratios.

The RIC protocol was also applied to *Arabidopsis thaliana*, requiring major adjustments to the challenges posed by plant tissue [13–15]. As plants contain UV absorbing pigments, the UV dosage for RNA-protein crosslinking in the tissue was increased. Moreover, stringent conditions for lysis were applied to overcome the hurdles by the rigid cell wall and the inherently higher RNase content of plant tissue (for review, see [16–18]). The RNA-binding proteome was profiled in different Arabidopsis tissues including leaves of four-week-old plants [13], leaf mesophyll protoplasts [14], etiolated seedlings [15], cell cultures derived from roots [13] or an egg-cell like callus [19]. Moreover, Bach-Pages and colleagues improved the purification conditions to more efficiently remove contaminations during oligo(dT) pulldown [20].

Collectively, these RIC approaches greatly advanced our understanding about the types of proteins capable of binding RNA, including many proteins lacking conventional RNA-binding domains or metabolic enzymes (reviewed in [11]). However, insights into the RBPome of a single RNA and its dynamic changes, which would yield mechanistic information on how RNA expression patterns are orchestrated, are scarce. Until recently, the identification of proteins interacting with a defined RNA or candidate regulatory regions within an RNA were mainly identified in vitro by immobilizing the RNA bait, incubating it with protein extracts from the tissue of choice and retrieving bound proteins for MS. For this, RNA can be chemically synthesized or in vitro transcribed in the presence of biotinylated UTP, allowing loading onto streptavidin beads [21]. Alternatively, RNAs can be spiked with a recognition sequence for a high affinity RBP such as the coat protein of phage MS2 [22]. Upon incubation of the MS2-tagged RNA with protein extracts of the tissue of choice, the assembled complexes are captured with immobilized MS2 coat protein-GFP and proteins co-purifying with the RNA are identified via MS [23]. To retrieve proteins regulating processing of miRNA precursors, a 16-nucleotide hairpin that is bound with high affinity by the cleavage deficient Csy4* Cas nuclease has been used as tag. The Csy4* protein is first immobilized onto beads followed by loading of an in vitro transcript comprising the miRNA precursor tagged with the hairpin sequence. After incubation with nucleoplasmic or cellular extracts, the protein-RNA complexes are retrieved by pulling down the Csy4*. Proteins are released by reactivation of the Csy4* cleavage activity and then subjected to MS [24, 25].

Overall, these in vitro approaches do not take into account features of the native environment including epitranscriptomic modifications of binding sites or interactions of RBPs with other molecules in the cell which may affect binding. Furthermore, the in vitro structure may not recapitulate the secondary structure found in the cell. Therefore, methods to capture proteins interacting with a single RNA species in vivo are needed.

Zooming in on a single RNA in vivo has been achieved for the 3.7 kb long human long noncoding RNA (lncRNA) NEAT1 (nuclear-enriched abundant transcript 1) and the 8 kb lncRNA MALAT1 (metastasis-associated lung adenocarcinoma transcript 1) [26, 27]. West and coworkers extended the Capture Hybridization Analysis of RNA Targets (CHART) procedure, originally designed to isolate lncRNAs bound to DNA from formaldehyde crosslinked tissue to identify sites of lncRNA interaction with genomic loci, to proteomics analysis by MS (CHART-MS) [28, 29]. Subsequent studies focused on the development of methods to comprehensively profile proteins interacting with the X-inactive specific transcript (Xist), a long noncoding RNA 17 kb in length required for X-chromosome inactivation and thus dosage compensation in female placental mammals. In a comprehensive identification of RBPs by mass spectrometry

(ChIRP-MS), Chu and co-workers employed long biotinylated antisense oligonucleotides (AOs) spanning the entire Xist transcript. After formaldehyde fixation of the tissue and preparation of lysates, these tiling AOs were hybridized to Xist under stringent conditions. Oligonucleotide-bound RNA and the in vivo assembled proteins were efficiently pulled down with streptavidin magnetic beads [30]. ChIRP-MS was also employed to recover proteins associated with human U1 and U2 snRNAs and Arabidopsis U1 snRNA [30, 31]. In RNA antisense purification (RAP)-MS, McHugh and co-workers used UV light for crosslinking, followed by hybridization with long biotinylated AOs under strong denaturing conditions [32]. Mass spectrometry identified a suite of RBPs that were functionally linked to chromatin spreading and silencing of Xist transcription [30, 32]. Pulldown with AOs designed against the lncRNA Pluripotency and Hepatocyte Associated RNA Overexpressed in HCC (PHAROH) identified the translational repressor TIAR that binds to a 71 nucleotide hairpin in PHAROH, leading to increased translation of MYC [33].

In Arabidopsis, Crespi and colleagues searched for proteins interacting with the *ALTERNATIVE SPLICING COMPETITOR* (*ASCO*) lncRNA, which has been shown to regulate the activity of the splicing regulator NUCLEAR SPECKLE RNA-BINDING PROTEIN a (NSRa) [34]. Pulldown with a set of 20-nucleotide long biotinylated AOs covering the length of the lncRNA identified the splicing factor PRP8, in line with the model of *ASCO* as a competitive inhibitor of the action of splicing factors [35].

A major drawback of these tiling approaches lies in the fact that they cannot distinguish between RNA isoforms or between closely related members of multigene families that are particularly prevalent in Arabidopsis. To increase the specificity, Rogell and colleagues modified the enhanced RIC protocol, using specific LNA/DNA AOs targeted at defined regions of a transcript and scrambled probes as control [36]. This "specific ribonucleoprotein (RNP) capture" procedure was tested against HeLa cell 18 S and 28 S ribosomal RNA and uncovered proteins previously unknown to interact with rRNAs or to be involved in rRNA biology.

Here, we explored RNA interactome capture in Arabidopsis to identify proteins interacting with a single mRNA that may contribute to processing and function of this mRNA. We chose the circadian-clock regulated transcript *AtGRP7* encoding a glycine-rich RNA binding protein as a paradigm, as it is one of the most abundant transcripts in Arabidopsis [37, 38]. In addition to transcriptional regulation by the circadian clock, *AtGRP7* is regulated at the posttranscriptional level. Elevated *At*GRP7 levels entail alternative splicing at a cryptic splice site in the intron leading to retention of the first half of the intron including a premature termination codon and, consequently, degradation via the Nonsense mediated decay pathway [39–42]. *At*GRP7 binds to its own pre-mRNA in vitro and in vivo [42–44] and mathematic modelling unveiled that this posttranscriptional regulation indeed contributes to the *AtGRP7* oscillations [45]. We hypothesize that additional proteins binding to the *AtGRP7* transcript in vivo contribute to shaping its temporal expression pattern.

An antisense oligonucleotide directed against the 5' untranslated region (UTR) proved most efficient in capturing *AtGRP7* transcript from lysates of UV crosslinked plants. Furthermore, the use of LNA oligonucleotides greatly enhanced the capture efficiency. The largest number of proteins were identified by two rounds of pulldown with the specific 5'UTR LNA oligonucleotide. Performing a tandem capture approach with the specific 5'UTR LNA oligonucleotide first followed by capture with an LNA oligo(dT) oligonucleotide led to an increased purity of the captured *AtGRP7* transcript but came at the cost of a reduced number of proteins detected in mass spectrometry. The proteins identified by the in vivo interactome captures were benchmarked against proteins recovered by in vitro pulldown using biotinylated, bead immobilized *AtGRP7* UTRs. Among the proteins interacting with the *AtGRP7* transcript both in vivo and in vitro was the family of ACETYLATION LOWERS BINDING AFFINITY (ALBA) proteins. Interaction of ALBA4 with the *AtGRP7* RNA was independently validated via individual-nucleotide resolution crosslinking and immunoprecipitation (iCLIP).

Overall, we adapted RNA interactome capture with LNA/DNA oligonucleotides to identify the complement of proteins interacting with a single mRNA in plants. We anticipate that further optimization and up-scaling of the protocol for transcripts of interest along with the continuous improvement of mass spectrometry sensitivity will further increase the detection proteins that are enriched relative to interactome capture from control plants devoid of the transcript of interest.

Methods

Plant lines

All Arabidopsis lines have the Col-0 background. The *grp7-1* T-DNA line was originally ordered from the Nottingham Arabidopsis stock centre (http:/arabidopsis.info; SALK_039556) and has been used in previous studies [46–49]. The *AtGRP7::AtGRP7-GFP* plants expressing the *At*GRP7-GFP fusion under control of 1.4 kb of the *At*GRP7 promoter and the *At*GRP7 5'UTR, intron and 3'UTR in the *grp7-1* T-DNA mutant have been described before [43, 47, 50, 51]. Both lines are available from Dorothee Staiger, Bielefeld University, Bielefeld, Germany, upon request.

The *alba456* triple mutant has been described previously [52]. Briefly, the *alba4* (SALK_015940), *alba5* (SALK_088909) and *alba6* (SALK_048337) T-DNA single mutants have been ordered from the Arabidopsis Biological Resource Center (ABRC) and combined by genetic crosses to yield the *alba456* triple mutant. The mutants are available from Anthony Millar, Australian National University, Canberra, Australia, upon request.

The transgenic line expressing the ALBA4-GFP fusion protein driven by 1.7 kb of the *ALBA4* promoter in the *alba456* triple mutant background, has been described and is available from Anthony Millar, ANU Canberra, Australia [52]. The transgenic 35 S-GFP line expressing GFP under control of the Cauliflower Mosaic Virus 35 S RNA promoter has been described and is available from Anthony Millar, Australian National University, Canberra, Australia, upon request [52].

Plant growth and UV crosslinking

Seeds were sterilized by chlorine gas (100 ml bleach and 3 ml 37% HCl) for 4 h in a sealed desiccator jar and germinated on half-strength Murashi Skoog plates [53]. Seedlings were grown in 16 h light-8 h dark cycles at 20 °C for 14 days. UV crosslinking was performed at zt13 (zeitgeber time 13, 13 h after lights on) at 2000 mJ/cm^2 [43, 54].

Probe design

LNA antisense oligonucleotides for *AtGRP7* were designed using the QIAGEN LNA Oligo Optimizer tool. Probes were designed to minimize self-complementarity of the sequence, secondary structure and no complementarity to other Arabidopsis transcripts, in particular the *AtGRP8* paralog. Furthermore, complementary regions in the *AtGRP7* transcript were selected that have little secondary structure as determined by the Vienna RNA fold server. Probes were 18–22 nts long with a melting temperature of 68–84°C and contained a flexible C6 linker carrying a primary amino group at the 3' end to couple them covalently to magnetic beads. All probes were HPLC purified.

LNA2.T are $(dT)_{20}$ oligonucleotides with every second dT substituted by an LNA-thymine [55].

Coupling of LNA oligonucleotides to magnetic beads

Probes were coupled to carboxylated magnetic beads (M-PVA C11, PerkinElmer, Waltham, MA, USA) in DNA/RNA low binding tubes. The oligonucleotides were resuspended in nuclease-free water (100 µM final concentration). The bead slurry (50 mg/ml) was washed three times with 5 volumes of 50 mM 2-(N-morpholino)ethanesulfonic acid (MES) pH 6.0. One volume of prewashed bead slurry was combined with 5 volumes of freshly prepared 20 mg/ml *N*-(3-dimethylaminopropyl)-*N'*-ethylcarbodiimide hydrochloride (EDC-HCl) in MES buffer and 0.66 volumes of the oligonucleotide solution (e.g. for 150 µl of bead slurry, 750 µl EDC-HCL solution and 10 nmol of probe in 100 µl H_2O were added). Coupling was performed for 5 h at 50 °C in a thermomixer (800 rpm). To monitor the coupling efficiency, the oligonucleotide concentration was measured in the supernatant by NanoDrop. Subsequently, the beads were washed 3 times with 2 ml 1x PBS pH 7.4 and residual free carboxyl residues were inactivated by adding 2 ml of 200 mM ethanolamine pH 8.5 for 1 h at 37 °C and 800 rpm in the thermomixer. The coupled beads were finally washed 3 times with 2 ml 1 M NaCl and stored in 0.1% (v/v) PBS-Tween at 4 °C until use.

Specific RNA interactome capture in vivo (medium- and large-scale experiments)

Above-ground tissue collected from 14 day old, UV crosslinked *grp7-1* or GRP7-GFP seedlings, respectively, was ground into a fine powder with liquid nitrogen. The following steps are described for 8 g of ground tissue, which were split up into two 50 ml tubes with 4 g each and resuspended in 25 ml lysis buffer (50 mM Tris-HCl pH 7.5, 500 mM NaCl, 0.5% SDS [w/v], 1 mM EDTA) supplemented with 1x protease inhibitor (complete EDTA free, Roche), 2.5% [w/v] polyvinylpyrrolidone 40 (PVP40), 1% beta-mercaptoethanol, 5 mM DTT and 10 mM Ribonucleoside Vanadyl Complex. The lysate was centrifuged for 12 min at 5000 rpm and 4 °C. The cell extract was then passed through a 0.45 µm filter and subsequently through a 27G needle to shear genomic DNA. In a fresh 50 ml tube, 42.5 ml cell extract were mixed with 7.5 ml formamide (15% (v/v) final concentration), and an aliquot of 100 µl was saved for RNA and protein analysis. For pre-clearing, 600 µl M-PVA C11 beads were equilibrated by washing three times in 3 volumes of lysis buffer and then added to 50 ml cell extract. After rotation for 1 h at 4 °C, the tubes were placed on a magnet for about 15 min at 4 °C and the cell extract was transferred to a new tube. For the specific RNP capture, 600 µl M-PVA C11 beads coupled to 40 nmol *AtGRP7* 5'UTR LNA oligo were washed three times in 3 volumes of lysis buffer, resuspended in 500 µl lysis buffer and heated up to 90 °C for 3 min to relax secondary structures. The beads were then added to 50 ml of cell extract and incubated for 2 h at 4 °C on a rotator. Tubes were then placed on a magnet and if a second round of capture was performed, the cell extract was transferred to a new tube and a fresh aliquot of beads coupled to the *AtGRP7* 5'UTR LNA oligo was added and incubated for 2 h at 4 °C with rotation. After hybridization and magnetic separation, a 100 µl aliquot of the cell extract was taken for RNA and protein analysis and the rest was discarded. Beads were resuspended in

2 ml of lysis buffer and transferred to a 2 ml DNA/RNA low binding tube. Beads were then washed four times in 2 ml 2 x SSC buffer supplemented with 0.5% SDS and 5 mM DTT followed by one wash with 2 ml 1 x SSC buffer (without SDS and DTT). All washes were carried out for 5 min at room temperature on a rotator. For pre-elution of unspecific binders, the beads were resuspended in 600 µl H_2O and incubated for 5 min at 40 °C and 800 rpm. After magnetic separation, the pre-eluates were saved for RNA and protein analysis. RNA-protein complexes were finally heat-eluted by resuspending the beads in 600 µl elution buffer (20 mM Tris-HCl pH 7.5, 1 mM EDTA) and incubation for 3 min at 90 °C and 800 rpm. Tubes were placed on a magnet, the eluates were transferred to a new tube and an aliquot was saved for RNA analysis. The rest of the eluate was either used for RNase treatment, protein concentration and western blot or mass spec, respectively, or subjected to another purification by oligo(dT) or LNA2.T capture.

For the medium-scale capture, this procedure was carried out with 32 g of ground tissue (8×4 g in 50 ml tubes) and for the large-scale capture, 100 g of ground tissue were used (24×4 g in 50 ml tubes) and the pre-eluates and eluates were pooled.

The preliminary test of capture efficiency of different LNA oligonucleotides was performed in the same way, except that only 12.5 ml of cell extract and 150 µl of beads coupled to 10 nmol of the respective LNA oligonucleotides were used.

LNA2.T capture

The pooled eluate from the capture with the *AtGRP7* 5'UTR LNA oligonucleotide (14.4 ml) was aliquoted into twelve 5 ml tubes with 1200 µl eluate each. This was mixed with 2667 µl elution buffer, 833 µl 3 M NaCl (final concentration of 0.5 M) and 300 µl of M-PVA C11 beads coupled to 20 nmol of LNA2.T oligo, which were first washed three times in 3 volumes of lysis buffer, resuspended in 300 µl lysis buffer and heated to 90 °C for 1 min. Hybridization was carried out for 2 h at 4 °C on a rotator. After magnetic separation for 10 min at 4 °C, the supernatant was transferred into a new tube and a second round of capture was performed with a fresh aliquot of LNA2.T coupled beads. Washes, pre-elution and elution were performed as described above, except that pre-elution and elution were carried out in a volume of 300 µl. Pre-eluates and eluates were pooled and used for quality controls and mass spec.

Recycling of beads coupled to LNA oligos

Beads coupled to LNA oligonucleotides can be reused multiple times and were recycled by resuspending them in 1 ml of nuclease-free water and incubation for 5–10 min at 95 °C and 800 rpm. Immediately afterwards, before bead slurry cool down, beads were collected by magnetic force, and the supernatant discarded. Beads were then washed 3 times with 5 volumes of water and 3 times with 5 volumes of lysis buffer and stored in 0.1% PBS–Tween at 4 °C until use.

To avoid cross-contamination, beads were only reused for the same line.

Oligo(dT) capture

The pooled eluate from the capture with the *AtGRP7* 5'UTR LNA oligo (2400 µl) was aliquoted into four 5 ml tubes with 600 µl eluate each. This was mixed with 3650 µl elution buffer (20 mM Tris-HCl (pH 7.5), 1 mM EDTA) and 500 µl 5 M LiCl (final concentration of 0.5 M). 240 µl of oligo(dT) bead slurry (New England Biolabs, Frankfurt, Germany) were washed three times in 1 ml of lysis buffer (20 mM Tris-HCl pH 7.5, 500 mM LiCl, 1 mM EDTA, 5 mM DTT, 0.5% (w/v) LiDS), resuspended in 250 µl elution buffer and then added to the eluate. Hybridization was carried out for 2 h at 4 °C on a rotator. After magnetic separation for 5 min at 4 °C, the supernatant was removed, and the beads were resuspended in lysis buffer and transferred to a 2 mL tube. Beads were then washed twice with 2 ml of buffer I (20 mM Tris-HCl pH 7.5, 500 mM LiCl, 1 mM EDTA, 5 mM DTT, 0.1% (w/v) LiDS), buffer II (20 mM Tris-HCl pH 7.5, 500 mM LiCl, 1 mM EDTA, 5 mM DTT) and buffer III (20 mM Tris-HCl pH 7.5, 200 mM LiCl, 1 mM EDTA, 5 mM DTT). Each wash was performed for 5 min at 4 °C on a rotator. To elute RNA-protein complexes, beads were resuspended in 400 µl elution buffer and incubated for 3 min at 50 °C and 800 rpm. Eluates were pooled and used for quality controls and mass spec.

Quality controls

RNA extraction, cDNA synthesis and qPCR

RNA was isolated from the input and the supernatant using commercial TRIzol (Thermo Fischer, Waltham, MA, USA) according to the manufacturer's instructions and RNA integrity was checked by denaturing agarose-formaldehyde gel electrophoresis. 4 µl of the RNA from input and supernatant and 7 µl of the pre-eluates and eluates were digested with RQ1 DNase I (Promega, Walldorf, Germany) and cDNA synthesis was carried out with Superscript IV reverse transcriptase (Thermo Fischer) and random hexamer primers according to the manufacturer's instructions. qPCR was performed in a volume of 10 µl with the iTaq SYBR GREEN supermix (Biorad, Hercules, CA, USA) using 45 cycles of 15 s at 95 °C and 30 s at 60 °C in a CFX96 cycler (Biorad). Primers are listed in Additional file 1.

RNase treatment, protein concentration and silver staining

The remainder of the pre-eluate and eluate was treated with RNase cocktail (Thermo Fischer) (0.5 µl per 1200 µl eluate/pre-eluate) for 1 h at 37 °C. After concentration using an Amicon filter device with a 3 K cut-off, the samples were subjected to SDS-PAGE using a 4–12% NuPAGE Bis-Tris gel run at 100 V in 1x MOPS buffer followed by silver staining as described in Reichel et al. [15].

Immunoblot analysis

Immunoblot analysis was done essentially as described in Meyer at el [43]. Primary antibodies were a polyclonal antibody against HISTONE 3 (Agrisera, Vännäs, Sweden, AS10710; rabbit; dilution 1:5000), and a monoclonal antibody against GFP (Roche, catalog number 11 814 460 001; mouse; dilution 1:1000). Secondary antibodies were HRP-coupled anti-rabbit IgG (Sigma-Aldrich catalog number A 0545; dilution 1:5000) or HRP-coupled anti-mouse IgG (Sigma-Aldrich catalog number A0168; dilution 1:2500). Chemiluminescence detection of the immunoblots was done with Fusion-FX6 system (Vilber Lourmat, Eberhardzell, Germany).

Mass spectrometry

Sample preparation

Reduction of disulfide bridges in cysteine containing proteins was performed with dithiothreitol (56 °C, 30 min, 10 mM in 50 mM HEPES, pH 8.5). Reduced cysteines were alkylated with 2-chloroacetamide (room temperature, in the dark, 30 min, 20 mM in 50 mM HEPES, pH 8.5). Samples were prepared using the SP3 protocol [56, 57] and trypsin (sequencing grade, Promega) was added in an enzyme to protein ratio of 1:50 for overnight digestion at 37 °C. The next day, peptides were recovered in HEPES buffer by collecting the supernatant a on magnet and combining it with the second elution wash of beads with HEPES buffer.

Peptides were labelled with TMT6plex [58] Isobaric Label Reagent (ThermoFisher) according to the manufacturer's instructions. Samples were combined for multiplexing and for further sample clean up an OASIS® HLB µElution Plate (Waters) was used. Offline high pH reverse phase fractionation was carried out on an Agilent 1200 Infinity high-performance liquid chromatography system, equipped with a Gemini C18 column (3 µm, 110 Å, 100×1.0 mm, Phenomenex, Aschaffenburg, Germany) [15].

LC-MS/MS

An UltiMate 3000 RSLC nano LC system (Dionex) fitted with a trapping cartridge (µ-Precolumn C18 PepMap 100, 5 µm, 300 µm i.d. x 5 mm, 100 Å) and an analytical column (nanoEase™ M/Z HSS T3 column 75 µm x 250 mm C18, 1.8 µm, 100 Å, Waters) was used. Trapping was carried out with a constant flow of trapping solution (0.05% (v/v) trifluoroacetic acid in water) at 30 µl/min onto the trapping column for 6 min. Subsequently, peptides were eluted via the analytical column running solvent A (0.1% (v/v) formic acid in water, 3% (v/v) DMSO) with a constant flow of 0.3 µl/min, with increasing percentage of solvent B (0.1% (v/v) formic acid in acetonitrile, 3% DMSO (v/v)). The outlet of the analytical column was coupled directly to an Orbitrap Fusion™ Lumos™ Tribrid™ Mass Spectrometer (Thermo Fischer) using the Nanospray Flex™ ion source in positive ion mode. The peptides were introduced into the Fusion Lumos via a Pico-Tip Emitter 360 µm OD x 20 µm ID; 10 µm tip (CoAnn Technologies) and an applied spray voltage of 2.4 kV. The capillary temperature was set to 275 °C. Full mass scan (MS1) was acquired with a mass range of 375–1500 m/z in profile mode in the orbitrap with a resolution of 60,000. The filling time was set to a maximum of 50 ms. Peptide fragmentation (MS) was performed using HCD, the Orbitrap resolution was set to 15,000, with a fill time of 54 ms and a limitation of 1×105 ions. A normalized collision energy of 36 was applied. MS2 data was acquired in profile mode.

Data analysis

IsobarQuant [59] and Mascot (v2.2.07) were used to process the acquired data, which was searched against a Uniprot *Arabidopsis thaliana* proteome database containing common contaminants and reversed sequences. The following modifications were included into the search parameters: Carbamidomethyl (C) and TMT10 (K) (fixed modification), Acetyl (Protein N-term), Oxidation (M) and TMT10 (N-term) (variable modifications). For the full scan (MS1) a mass error tolerance of 10 ppm and for MS/MS (MS2) spectra of 0.02 Da was set. Further parameters were set: Trypsin as protease with an allowance of maximum two missed cleavages: a minimum peptide length of seven amino acids; at least two unique peptides were required for a protein identification. The false discovery rate on peptide and protein level was set to 0.01.

The raw output files of IsobarQuant (protein.txt – files) were processed using the R programming language [60]. Contaminants were filtered out and only proteins that were quantified with at least two unique peptides were considered for the analysis. 18 (Fig. 3D), 63 (Fig. 4A), 386 (Fig. 4C) and 2626 (Fig. 6E) proteins passed these criteria. Raw TMT reporter ion intensities ('signal_sum' columns) were used for further analysis. For Figs. 3D and 4C, GRP7-GFP and *grp7-1* fold-changes were calculated on raw TMT reporter ion intensities. For Fig. 4A, raw TMT reporter ion intensities were normalized using vsn before (variance stabilization normalization [61]). For Fig. 6E, raw TMT reporter ion intensities were first cleaned for batch effects using limma [62] and further

normalized using vsn [61]. Proteins were tested for differential expression using the limma package. The replicate information was added as a factor in the design matrix given as an argument to the 'lmFit' function of limma. A protein was annotated as a hit with a false discovery rate (fdr) smaller 0.05 and a $\log_2$ fold-change of at least 1.

In vitro pulldowns

Isolation of nucleoplasmic proteins

14-day old Col-0 seedlings were snap-frozen in liquid nitrogen and ground into a fine powder by mortar and pestle. 5 g of ground material were resuspended in 15 ml lysis buffer (20 mM Tris-HCl pH 7.5, 25% (v/v) glycerol, 20 mM KCl, 2 mM EDTA, pH 8.0, 2.5 mM $MgCl_2$, 250 mM sucrose, 5 mM DTT) [24]. The suspension was filtered through a 100 µm mesh and 2 layers of miracloth. The sample was diluted to 50 ml with lysis buffer and centrifuged at 1500 × g for 30 min at 4 °C. The crude nuclear pellet was resuspended in 12 ml NRBT (20 mM Tris-HCl pH 7.4, 25% (v/v) glycerol, 2.5 mM $MgCl_2$, 0.2% Triton X-100), incubated on ice for 3 min and centrifuged at 1500 × g for 30 min at 4 °C. This washing step was repeated 5 to 6 times until the pellet was whitish. Finally, the pellet was suspended in 3 volumes (~600 µl) of protein extraction buffer (20 mM Hepes-KOH, pH 7.5, 5% (v/v) glycerol, 1.5 mM $MgCl_2$, 0.2 mM EDTA pH8.0, 420 mM NaCl, 5 mM DTT, 1x Complete Protease inhibitor (Roche, San Francisco, CA, USA) [63] and adjusted to 150 mM NaCl.

In vitro transcription

The template for the 5'UTR was PCR amplified from a plasmid harbouring the *AtGRP7* 5'UTR and 15 nucleotides of exon 1 driven by the T7 promoter using primers gB_5'UTR_t7_fwd and gB_5'UTR_rev (Additional file 1). The template for the 3´UTR was PCR amplified from a plasmid harbouring the *AtGRP7* 3'UTR driven by the T7 promoter using primers gB T7 GRP7 3'UTR fwd and gB T7 GRP7 3'UTR rev (Additional file 1). PCR products were purified using the NucleoSpin Gel and PCR Clean-up (Macherey-Nagel) and used for in vitro transcription.

In vitro transcription was performed using the MEGAshortscript T7 transcription kit (Invitrogen, Carlsbad, CA, USA) according to the manufacturer's instructions with a mixture of Biotin 11-UTP and UTP so that each transcript contained on average three biotinylated uracil. The in vitro transcripts were purified using the RNA Clean & Concentrator-25 Kit (Zymo Research, Freiburg, Germany) and analyzed via Urea-PAGE.

Coupling of in vitro transcripts to magnetic beads

50 pmol of the biotinylated in vitro transcripts were diluted in 2x folding buffer (40 mM Tris-HCl pH 7.5, 200 mM NaCl, 6 mM $MgCl_2$), incubated at 70 °C for 10 min, put on ice for 1 min and incubated at room temperature for 10 min. An aliquot was taken as input. Thirty µl of magnetic Dynabeads MyOne Streptavidin beads were washed in 1x folding buffer and incubated with the renatured in vitro transcripts at 4 °C for 1.5 to 2 h. Beads were placed on a magnet and an aliquot of the supernatant was taken to monitor coupling efficiency. Additionally, 5% of the beads were used to elute the RNA in formamide containing loading dye (90% formamide, 10% glycerol, bromophenol blue, xylene cyanol) and check the RNA integrity on the beads before pulldown by urea PAGE.

Capture of RNA-protein complexes

The rest of the beads was incubated with 2 ml (ca. 800–1000 µg) nucleoplasmic protein extract for 2 h at 4 °C in an end-over-end rotator. Subsequently, beads were placed on a magnet, an aliquot of the supernatant was taken for protein analysis and the rest was discarded. The beads were washed three times with 500 µl protein wash buffer (20 mM Tris-HCl pH 7.5, 100 mM NaCl, 5% (v/v) glycerol, 1 mM TCEP, 0.1% Triton X-100) for 5 min at 4 °C and 800 rpm. 5% of the beads were used to elute the RNA with formamide containing loading dye and check the RNA integrity after the pulldown by urea PAGE. Proteins were eluted from the remaining 95% of the beads by resuspending them in 40 µl 1x LDS sample buffer (Thermo) and incubation for 10 min at 70 °C. Proteins were either analysed by silver staining or mass spectrometry. A pulldown with empty beads was performed side-by-side as a negative control. Four replicates were processed in parallel and analysed by mass spec.

Mass spectrometry

For the pulldown with the 5'UTR, samples were processed as described for the in vivo pulldowns.

The 3'UTR samples were measured with an EasyLC/Q Exactive Plus mass spectrometer platform as described [24]. The data was analysed as described for the in vivo pulldown.

GO term analysis

Genes enriched in gene ontology (GO) terms were analyzed in the online Thalemine database using the default background population and Holm–Bonferroni test correction.

Circadian time course

Col-0 wild-type plants and the *alba456* mutant were grown on half strength MS medium in entraining long day conditions at 20°C for 12 days before shifting them

to continuous light (LL). Plants were harvested at two-hour intervals in long days and from 28 to 76 h after transfer to LL. Plants were flash frozen in liquid nitrogen and RNA was isolated using the Universal RNA purification kit (Roboklon, Berlin, Germany). cDNA synthesis was performed with 1 µg RNA and AMV reverse transcriptase (Roboklon) using oligo(dT) primers according to manufacturer's instructions. qPCR was performed in a volume of 10 µl with the iTaq SYBR GREEN supermix (Biorad) using 45 cycles of 15 s at 95°C and 30 s at 60°C in a CFX96 cycler (Biorad). Data were normalized to the transcript encoding the PP2A subunit A3 (At1g13320) and expressed as the mean of two biological replicates ± SEM. Primers are listed in Additional file 1.

Results

Experimental strategy and evaluation of different probes for specific RNP capture

To enable identification of proteins that interact with a defined mRNA in vivo, we adapted the procedure for specific ribonucleoprotein capture developed by Rogell et al. [36] for ribosomal RNAs for the use in plants, employing the *AtGRP7* (AT2G21660) mRNA as proof-of-concept [36].

To find the optimal antisense probe, we designed multiple oligonucleotides targeting different regions of the *AtGRP7* transcript (5'UTR, 3'UTR, and exon 2) according to established LNA design guidelines using the QIAGEN LNA Oligo Optimizer tool. Probes were 18–22 nt long and had a melting temperature of ~70–80 °C (Fig. 1A). The sequences of the probes were designed to have little self-complementarity, no strong secondary structures, and no complementarity to other transcripts in Arabidopsis (especially to the paralogous *AtGRP8*). Additionally, probes were designed to target regions of the *AtGRP7* transcript that do not contain strong secondary structures, as determined by the Vienna RNAfold web server. At the 3' end, probes contained a flexible C6 linker and a primary amine, which allows covalent coupling to carboxylated magnetic beads (Fig. 1B). Covalent coupling enables the use of high concentrations of salts and detergents for stringent purification of the RNPs, and the recycling of capture probes, which saves costs. Using the protocol by Rogell et al. [36] as a starting point, we systematically optimized the conditions for cell lysis, probe hybridization, removal of unspecific binders and elution for plants.

As starting material, we used 14-day-old seedlings expressing *At*GRP7-GREEN FLUORESCENT PROTEIN (GFP) under the endogenous promoter in the *grp7-1* background with the rationale to monitor the pulldown of *At*GRP7 known to interact with its own transcript by immunoblotting with the GFP antibody. Seedlings were UV-crosslinked at 2000 mJ/cm^2 as established for our individual-nucleotide resolution crosslinking and immunoprecipitation (iCLIP) protocol [43, 64]. First, we compared the capture efficiency of the LNA probes directed against different transcript regions (Fig. 1A). To perform the capture, a cell extract was prepared by homogenizing 2 g of plant tissue in 12.5 ml of lysis buffer. The cell extract was then cleared by centrifugation and filtered through a 0.45 µm filter. Probes were coupled to the magnetic beads and heated to 90 °C for 3 min before hybridization to relax possible secondary structures. Formamide was added to the cell extract to a final concentration of 15% (v/v) to decrease the melting temperature of the probe-RNA duplex and thereby decrease unspecific binding. Hybridization was carried out for 2 h at 4 °C under constant rotation. After magnetic separation and removal of the supernatant, beads were washed multiple times followed by a pre-elution step with H_2O at 40 °C for 5 min to remove non-specifically bound transcripts. Finally, RNA-protein complexes were heat-eluted at 90 °C for 3 min.

First, we checked for the ability of the oligonucleotides to capture the *AtGRP7* transcript by assessing transcript levels in the input, pre-eluates and eluates using RT-qPCR. The first LNA oligo directed against the 5'UTR (termed 5'UTR_1) clearly performed best, as it captured about 70% of the *AtGRP7* RNA present in the input, while at the same time capturing only small amounts of other transcripts such as *AtGRP8* or the highly abundant *UBQ10* mRNA or 18 S rRNA (Fig. 1C). Interestingly, the performance of the second LNA oligo directed against the 5'UTR (termed 5'UTR_2) was considerably worse, even though located in a similar region. The LNA oligo targeting exon2 managed to capture almost 60% of the *AtGRP7* RNA present in the input but was less specific as it also captured more *AtGRP8* transcript. In contrast, the LNA oligos targeting the 3'UTR failed to efficiently capture *AtGRP7* with transcript levels in the eluates not being significantly different to those of the scrambled control. Importantly, the pre-elution step successfully removed unspecific binders (Fig. 1C). Subsequently, we checked whether we pulled down proteins bound to the *AtGRP7* transcript. We performed a capture experiment using the 5'UTR_1 LNA oligo and cell extracts from UV crosslinked *At*GRP7-GFP plants or *grp7-1* mutants as a control, respectively. Western blot analysis showed that the *At*GRP7 protein, which is known to bind to its own transcript, could be efficiently enriched in the eluate of the *At*GRP7-GFP sample, while being absent in the mutant (Fig. 1D) (Additional file 2, Fig. S1: Uncropped blots to Fig. 1). The abundant DNA-binding protein Histone H3 served as a negative control and was absent in the eluates from both *At*GRP7-GFP and *grp7-1* samples. Together, this demonstrated that the 5'UTR_1 LNA

(A)

Glycine-rich protein 7 (AtGRP7)-GFP

Oligonucleotide	Sequence (5'-> 3')	Length	Probe position	# LNA bases	T_m probe-RNA hybrid
GRP7_5'UTR_1	GTAGTGAGCAGTGAGATGTG	20 nt	184	6	84
GRP7_5'UTR_2	AAGGGATTACAGTGAGAGTA	20 nt	201	6	81
GRP7_exon2	CTCCACCCTCGCGTCTAC	18 nt	609	5	84
GRP7_3'UTR_2	GAAGAAATTTGTTATTTAGAGA	22 nt	944	6	68
GRP7_3'UTR_3	ATCAATCAACAGAGATAATA	20 nt	971	6	71
Scramble	GATATAGGATAGAATGCGAG	20 nt	-	6	78

(B)

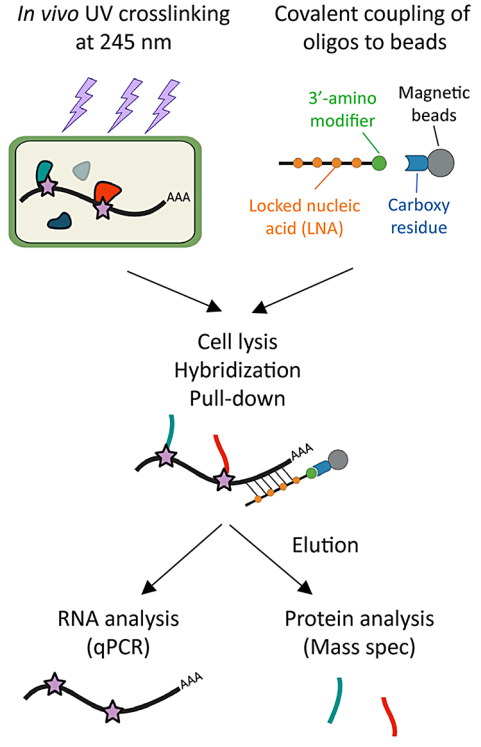

(C)

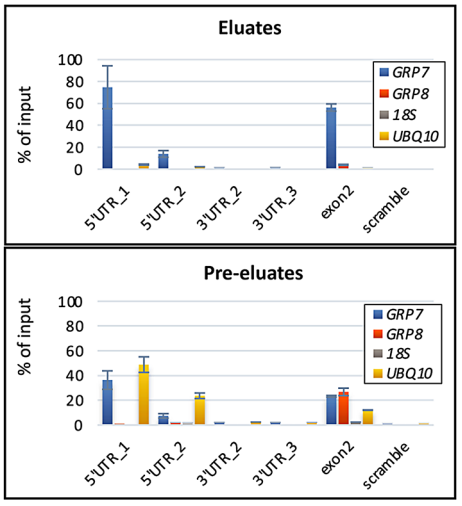

(D)

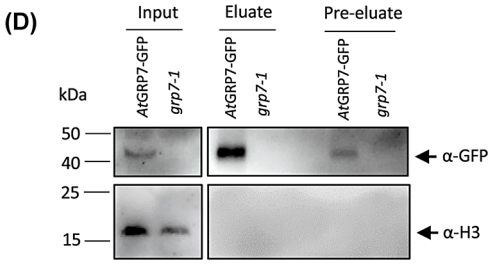

Fig. 1 Principle of the *AtGRP7* RNA interactome capture. **(A)** Scheme of the *AtGRP7-GFP* mRNA and details of the antisense LNA/DNA mixmer oligonucleotides tested for capture of the *AtGRP7* transcript. LNA nucleotides are underlined. The probe position is indicated relative to the TAIR cDNA sequence. **(B)** Principle of the specific RNP capture. 14-day-old seedlings are crosslinked with 254 nm UV light to establish covalent bonds between RNA and proteins. The LNA oligonucleotides are coupled to carboxylated magnetic beads via a primary amine attached to a C6 linker at their 3'end. Cell lysates are incubated with the bead-coupled oligonucleotides to pull down proteins interacting with the *AtGRP7* RNA. RNA-protein complexes are eluted and either subjected to RNA analysis via RT-qPCR or to protein analysis via mass spectrometry. **(C)** Capture efficiency and specificity with the different LNA/DNA mixmer oligonucleotides. Captures were performed with UV crosslinked *AtGRP7*::*At*GRP7-GFP (*grp7-1)* seedlings and RNA levels of *AtGRP7*, *AtGRP8*, 18 S rRNA and *UBIQUITIN 10* were measured in the eluates (top panel) and pre-eluates (bottom panel) by RT-qPCR using the primers listed in Additional file 1. Transcript levels are expressed relative to the transcript level in the input. **(D)** Immunoblot analysis of *AtGRP7*::*At*GRP7-GFP *grp7-1* and *grp7-1* control plants subjected to RNP capture with 5'UTR_1 LNA oligonucleotides. The lysate (input), pre-eluate, and eluate fractions were probed with the α-GFP antibody (top) or the α-Histone H3 antibody (bottom)

probe is able to efficiently capture *AtGRP7* RNA and associated binding proteins.

Improved capture efficiency by implementation of tandem capture, optimized buffer conditions and removal of genomic DNA

When transcript levels in the eluate were compared relative to the input, the 5'UTR_1 LNA probe efficiently captured *AtGRP7* RNA (Fig. 1C); however, when comparing levels of different transcripts in the eluate, it becomes apparent that the most abundant RNA species present is 18 S rRNA (Fig. 2A). To tackle this issue, we performed a tandem-capture approach similar to the study by Matia-Gonzáles et al. [65], where we first used oligo(dT) beads to enrich for all polyadenylated RNAs, followed by specific capture of *AtGRP7* with the 5'UTR_1 LNA probe. Although this could remove some of the 18 S rRNA, it still remained the most abundant species in the eluate (Fig. 2B). Interestingly, when we performed the tandem capture the other way around (specific capture followed by oligo(dT)), we could successfully remove the vast majority of ribosomal RNA and other unspecific transcripts, specifically enriching for *AtGRP7* (Fig. 2C).

However, we noticed some degree of RNA degradation in the lysate, which decreased the amount of transcript present to be captured (Additional file 3). Therefore, we aimed to further optimize the protocol by comparing the lysis and wash buffers that we use here [36] to the ones used in ChIRP-MS [30]. For this comparison, we performed a pulldown employing the ChIRP buffers with small adjustments (Additional file 3). The ChIRP lysis buffer contained NaCl and SDS instead of LiCl and LiDS, and 1 mM EDTA instead of $MgCl_2$. Washes were carried out with 2x SSC and 1x SSC buffer, while the wash buffers in Rogell et al. [36] had the same composition as the lysis buffer but with decreasing concentrations of salt

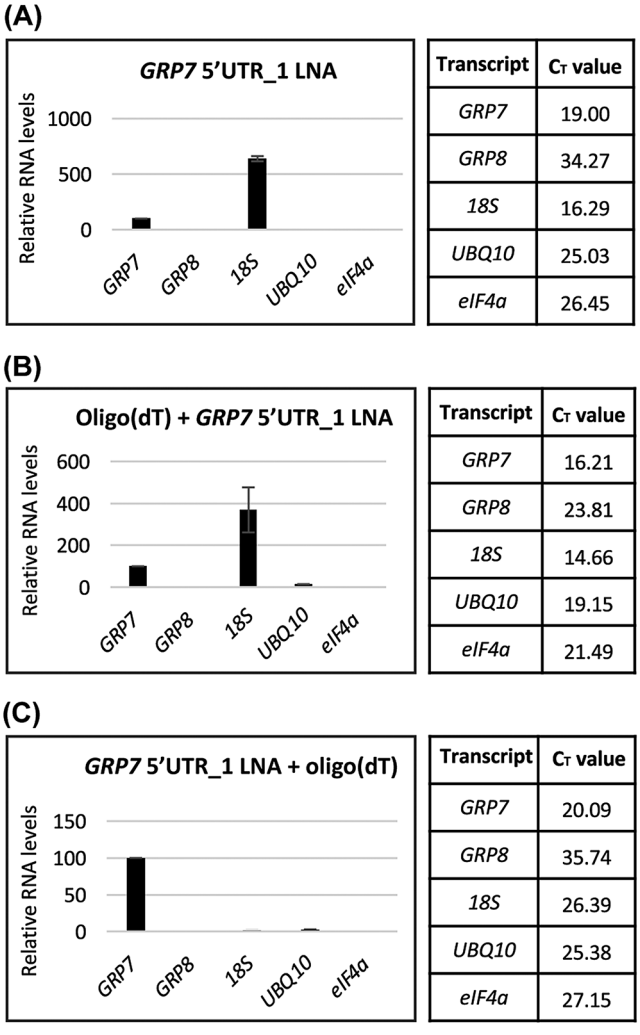

Transcript	C_T value
GRP7	19.00
GRP8	34.27
18S	16.29
UBQ10	25.03
eIF4a	26.45

Transcript	C_T value
GRP7	16.21
GRP8	23.81
18S	14.66
UBQ10	19.15
eIF4a	21.49

Transcript	C_T value
GRP7	20.09
GRP8	35.74
18S	26.39
UBQ10	25.38
eIF4a	27.15

Fig. 2 Optimization of the capture efficiency for the LNA 5'UTR_1 probe by tandem capture with oligo(dT). Relative RNA levels in the eluates after a single round of RNP capture with LNA 5'UTR_1 (**A**), tandem capture with oligo(dT) followed by the LNA 5'UTR_1 probe (**B**), and tandem capture with the LNA 5'UTR_1 probe followed by oligo(dT) capture (**C**). The *AtGRP7* level is set to 100%

and detergents (Additional file 3). Both the RNA integrity in the cell lysate and the capture efficiency as assessed by RT-qPCR could be significantly improved with the ChIRP buffers (Additional file 3) (Additional file 2, Fig. S2: Uncropped gels to Additional file 3). Hence, these buffers were used for all subsequent experiments.

Additionally, the cell lysate was passed once through a 27G needle before probe hybridization to shear genomic DNA (gDNA) and avoid its binding to the probes. RT-PCR of *AtGRP7* using primers that span the intron and can detect both gDNA and mRNA (Additional file 4) showed that only a small amount of gDNA was present in the eluate after capture, even without DNA shearing. However, inclusion of this step eliminated the last traces of gDNA to a non-detectable level. Moreover, shearing gDNA led to higher levels of captured *AtGRP7* mRNA, while at the same time not increasing the amount of non-specifically bound transcripts (Additional file 4) (Additional file 2, Fig. S3: Uncropped gels to Additional file 4).

Medium-scale tandem RNA interactome capture only identifies few interacting proteins

After having improved the protocol, we next performed a tandem capture (specific capture with 5'UTR_1 LNA probe followed by oligo(dT)) on a medium scale using 32 g of ground plant material from UV crosslinked *At*GRP7-GFP plants or the *grp7-1* mutant as a control. Denaturing RNA gel electrophoresis (Fig. 3A) and silver staining (Fig. 3B) (Additional file 2, Fig. S4: Uncropped gels to Fig. 3) showed that RNA and proteins were intact before and after probe hybridization, indicating that there was no degradation during the capture. RT-qPCR analysis demonstrated that *AtGRP7* RNA was specifically enriched over other RNAs in the eluate from the *AtGRP7*-GFP sample and was absent in the *grp7-1* eluate, which contained mostly ribosomal RNA (Fig. 3C). Despite these quality controls looking promising, the MS analysis only returned 18 proteins in total that were quantified (Additional file 5). Since this experiment was performed with only one replicate due to the large amount of starting material required, we chose a very stringent cut-off of a $\log_2$ fold-change (FC) ≥ 2 for a protein to be considered significantly enriched. Of the quantified proteins, only *At*GPR7 fulfilled this criterion (Fig. 3D). Gene ontology (GO) term analysis showed that the identified proteins were enriched in RNA-related terms (Fig. 3E), suggesting that the capture protocol per se is working, but needed further optimization and up scaling.

Further optimization by two consecutive captures and replacement of oligo(dT) with LNA2.T probes

To increase the number of RNA-protein complexes in the eluate, we decided to perform two consecutive rounds of capture from the same cell extract with the 5'UTR_1 LNA oligo by using the supernatant after the first hybridization as input for the second round of hybridization with a fresh aliquot of bead-coupled oligonucleotides. Analysis of RNA and proteins after round 1 and round 2 demonstrated that the prolonged time of the protocol did not lead to degradation (Additional file 6) (Additional file 2, Fig. S5: Uncropped gels to Additional file 6). Furthermore, *AtGRP7* RNA could also be efficiently enriched after the second round of capture (Additional file 6).

We also introduced a pre-clearing step with empty beads to reduce unspecific binding. Additionally, we substituted the oligo(dT) beads with 20-mers bearing an LNA-thymine at every other position (LNA2.T), which has been shown to be superior to standard oligo d(T) oligonucleotides for poly(A) RIC [55].

Identification of AtGRP7 interacting proteins with optimized large-scale RNA interactome capture

Scaling up the starting material from 32 g to 100 g of UV-crosslinked, ground *At*GPR7-GFP and *grp7-1* tissue, respectively, we performed another tandem capture with two rounds of capture with the 5'UTR_1 LNA oligo followed by two rounds of LNA2.T capture, and analyzed the samples by MS. Compared to the previous medium-scale experiment with 32 g of tissue, the total number of quantified proteins was increased to 63, of which 33 had a positive fold change. *At*GRP7 again showed the highest $\log_2$ fold-change (Fig. 4A, Additional file 5). Although the tandem capture has the advantage of specifically enriching for *AtGRP7* RNA in the eluate while removing most of the contaminating transcripts (Additional file 7), much of the *AtGRP7* transcript is lost during this stringent, multi-step procedure with only less than 20% of the input being present in the eluate (Fig. 4B).

Since this is limiting the number of captured proteins, we repeated the large-scale experiment with 100 g of tissue but did not include the LNA2.T capture. This increased the level of *AtGRP7* transcript in the eluate to about 60% of the input (Fig. 4D), but with the downside of also increasing the amount of nonspecifically bound transcripts, most notably ribosomal RNA (Additional file 7). However, since these unspecific transcripts are also present in the *grp7-1* control (Additional file 7), we reasoned that associated proteins would not be significantly enriched in the MS. Omitting the LNA2.T capture increased the number of proteins to 386 with 356 having a positive fold change and three, including *At*GRP7, having a $\log_2$ fold-change of at least 2 (Fig. 4C, Additional file 5). To validate our MS data, we analyzed the identified proteins from both large-scale (single and tandem) captures by GO term analysis, where we included all proteins with a positive fold change. Although the ones without significant enrichment do not pass the statistical criteria and therefore cannot be clearly distinguished

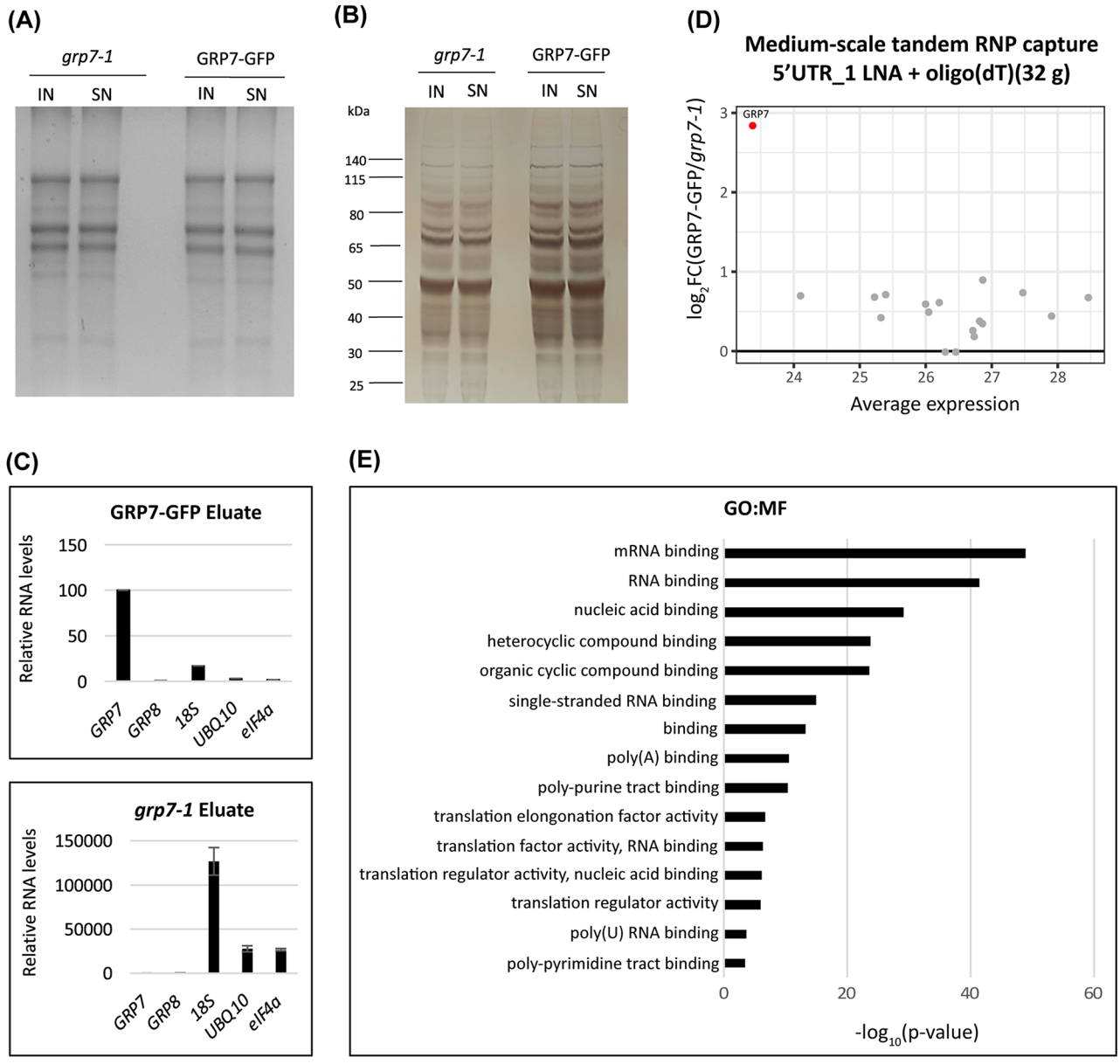

Fig. 3 Mass spectrometry analysis of proteins bound to the *AtGRP7* transcript after medium-scale tandem capture. **(A)** Agarose-formaldehyde gel electrophoresis of total RNA in the lysate (input) and the supernatant after probe hybridization (SN) in *AtGRP7*-GFP *grp7-1* plants and *grp7-1* control plants. **(B)** Silver staining of total protein in the lysate (input) and the supernatant after probe hybridization (SN) in the *AtGRP7*-GFP *grp7-1* plants and *grp7-1* control plants. The positions of the molecular weight markers are indicated. **(C)** Relative RNA levels of *AtGRP7*, *AtGRP8*, 18 S rRNA, *UBIQUITIN10*, and *eIF4a* RNA in the eluates of *AtGRP7*-GFP *grp7-1* plants (top) and *grp7-1* control plants (bottom). **(D)** MA plot of identified proteins displaying the relation between $\log_2$ fold-change and the average expression (as $\log_2$ TMT signal). The *At*GRP7 protein was significantly enriched (red dot). **(E)** GO term analysis of the molecular function of the proteins identified

from unspecific binders, they likely contain interesting candidates for further analysis. Indeed, molecular function (MF) GO terms for both large scale captures were linked to RNA-related terms, most notably (m)RNA binding and nucleic acid binding (Fig. 4E-F). Similarly, the top 10 enriched biological process (BP) GO terms were connected to RNA (Fig. 4G-H).

When comparing the proteins with a positive fold change from the large-scale tandem and single RNP captures, we found that almost all proteins (30 out of 33) from the tandem capture were also present in the single capture (Fig. 5A). In this set of common 30 proteins (Additional file 8) almost all of them contained known RNA-binding domains (RBDs), with the RRM domain being the most abundant one (Fig. 5B). Moreover, we performed a STRING network analysis and found that these proteins contain many interaction nodes (Fig. 5C), suggesting that they may be functionally linked in

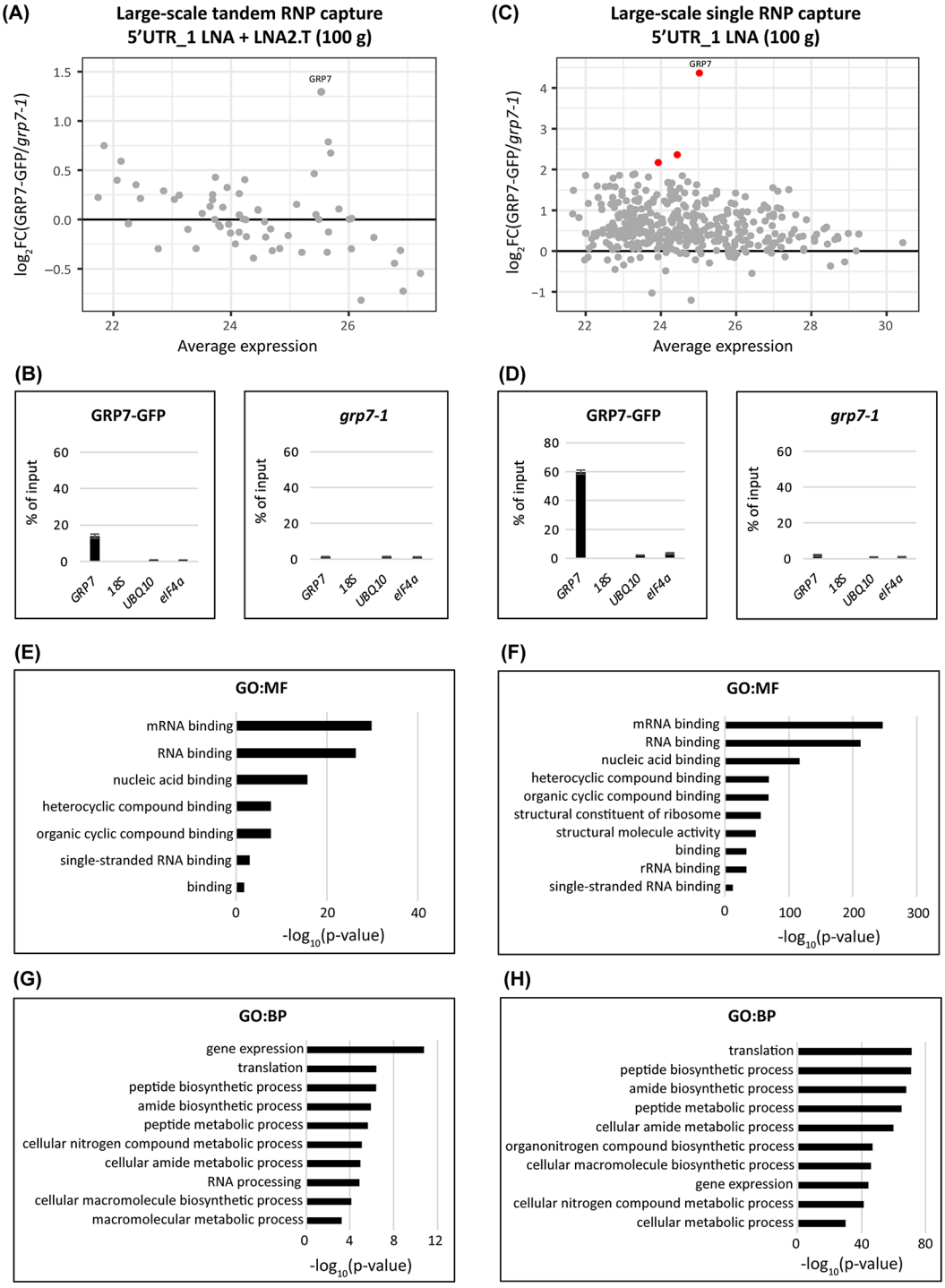

Fig. 4 Mass spectrometry of proteins binding to the *AtGRP7* transcript after large-scale capture. MA plot of identified proteins (**A, C**), relative RNA levels of *AtGRP7*, 18 S rRNA, *UBIQUITIN 10*, and *eIF4a* in the eluates of *AtGRP7*-GFP *grp7-1* plants (left) and *grp7-1* control plants (right) (**B, D**) and enriched GO terms of identified proteins **(E** and **G, F** and **G**) after large-scale tandem capture with two consecutive rounds of hybridization with the 5'UTR_1 LNA oligo followed by LNA2.T capture, or after large-scale single capture with two consecutive rounds of hybridization with the 5'UTR_1 LNA oligo only. Proteins with a $\log_2$ fold-change ≥ 2) are indicated by the red dots

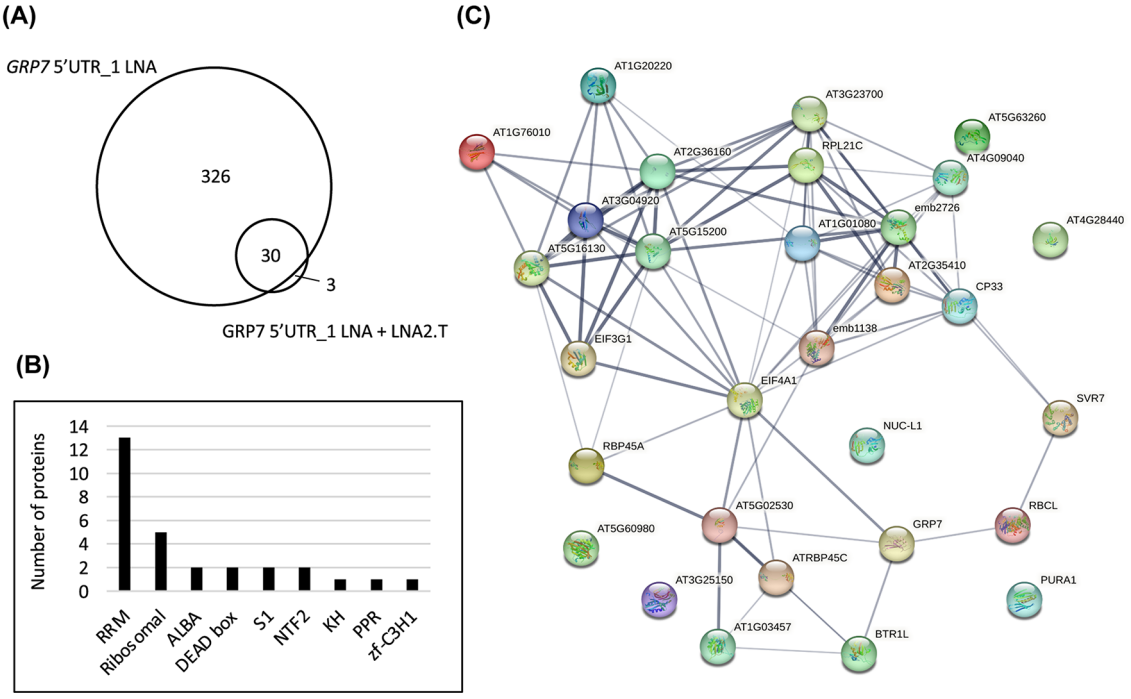

Fig. 5 Properties of proteins with a positive fold-change after large-scale RNP capture. **(A)** Venn diagram showing the overlap between the proteins identified in the large-scale single capture with two consecutive rounds of hybridization with the 5'UTR_1 LNA oligo and the large-scale tandem capture with hybridization with 5'UTR_1 LNA oligo followed by LNA2.T capture. **(B)** Number of proteins annotated with classical RNA-binding domains among the 30 common proteins. (**C)** STRING network analysis of the 30 common proteins

support of authentic interactions. Taken together, these results show that even though we find only few proteins enriched upon pulldown in *At*GRP7-GFP plants relative to the *grp7-1* control, our in vivo approaches using LNA oligonucleotides were nevertheless able to strongly enrich for proteins know to be involved in RNA binding and potentially function as novel regulators of *AtGRP7*.

Identification of proteins interacting with AtGRP7 UTRs by in vitro RNA interactome capture

The proteins recovered by specific capture of *AtGRP7*in vivo were compared to a set of proteins identified by in vitro pulldowns of the *AtGRP7* 5'UTR and 3'UTR. These regions were chosen because we obtained extensive crosslinking of the *At*GRP7 protein to these regions in iCLIP [43].

As a bait, we used in vitro transcribed, biotinylated RNA of the *AtGRP7* 5'UTR and 3'UTR, respectively, coupled to magnetic Dynabeads MyOne Streptavidin beads. The 3'UTR RNA bait contained the annotated 3'UTR sequence, and the 5'UTR RNA bait contained the 5'UTR sequence including the transcription start site [44] and 15 nucleotides of the first exon (Additional file 9). These bait RNAs were incubated with nucleoplasmic extracts prepared from 5 g of ground 14-day old Col-0 wild-type plants to avoid contamination with the highly abundant DNA-binding proteins coming from the chromatin. Unspecific background was minimized by washing the immobilized RNA–protein complexes three times with buffer containing 100 mM sodium chloride and 0.1% Triton X-100 as a non-ionic detergent. RNA-protein complexes were then recovered by heat-elution in LDS sample buffer. A pulldown with empty beads served as negative control.

We first performed a test pulldown to check RNA integrity after different steps of the protocol. As demonstrated by urea PAGE, the 5'UTR and 3'UTR bait RNAs were efficiently coupled to the beads, as they were depleted in the supernatant (SN) after coupling (Fig. 6A and B) (Additional file 2, Fig. S6: Uncropped gels to Fig. 6). Importantly, both bait RNAs were intact before and after the pulldown (Fig. 6A and B). Silver staining showed that our in vitro capture approach could enrich for specific proteins as compared to the empty beads control (Fig. 6C and D) (Additional file 2, Fig. S6: Uncropped gels to Fig. 6). We then performed four biological replicates for each capture and analyzed the proteins by MS. Capture with the 5'UTR and 3'UTR RNA baits identified 213 and 356 proteins, respectively, that were significantly enriched over empty beads, using the standard cut-off of a $\log_2$FC≥1 and a p-value≤0.05 (Fig. 6E, F). For both pulldowns, the GO terms of these proteins were strongly enriched in RNA-related terms, validating our in vitro approach (Additional file 10).

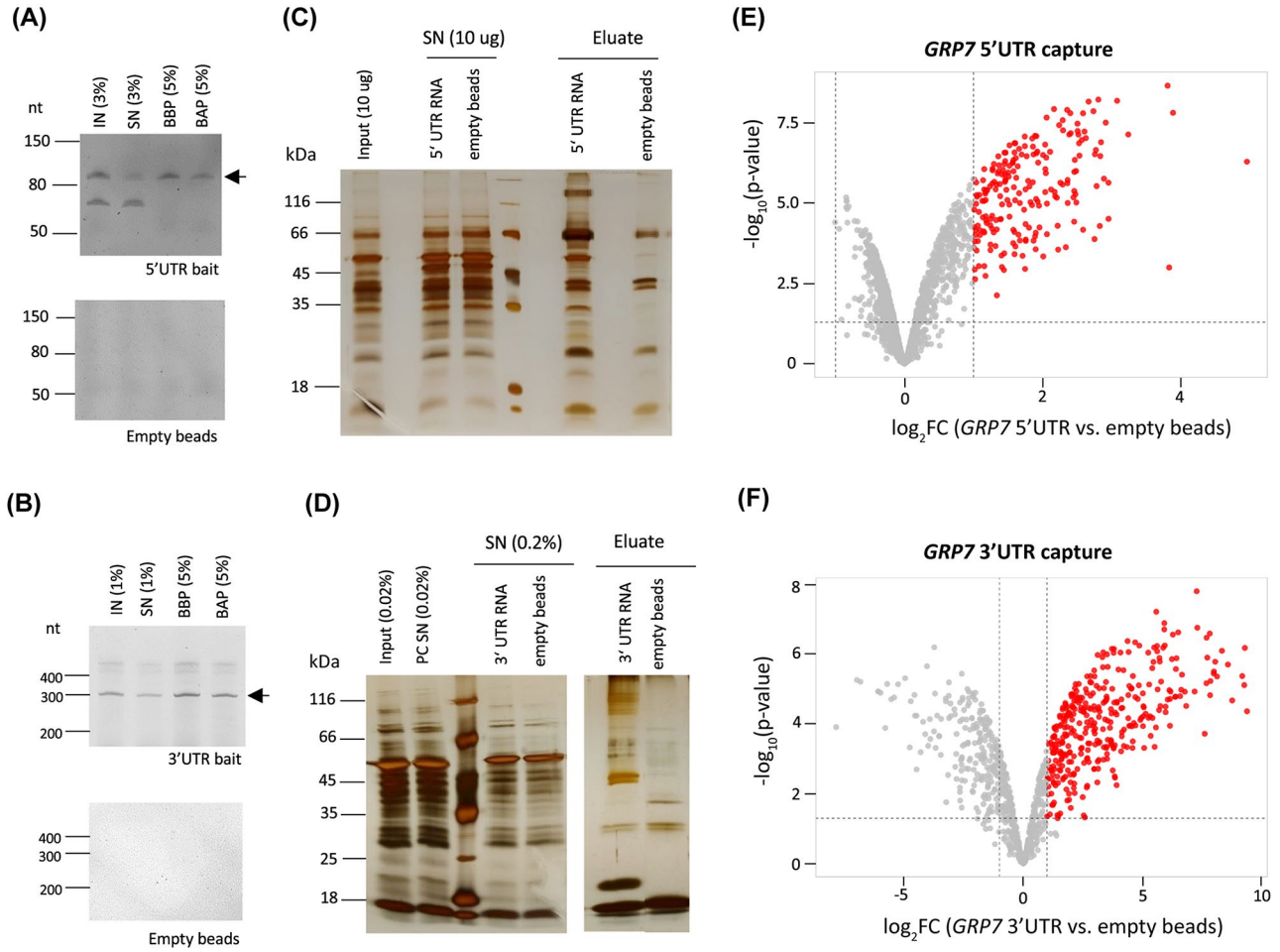

Fig. 6 Identification of *AtGRP7* binding proteins by in vitro pulldowns. **(A, B)** Coupling efficiency of biotinylated 5'UTR bait (**A**) and 3'UTR bait (**B**) to magnetic streptavidin beads. Aliquots of the RNA isolated from the input (IN), supernatant after coupling (SN) and eluates from the beads before (BBP) and after pulldown (BAP) were analyzed on 12.5% urea PAGE gels. Empty beads were used as controls. The arrows indicate the in vitro transcripts of the sizes expected for the 5'UTR (**A**) or 3'UTR (**B**), respectively. The additional bands likely represent additional conformations. **(C, D)** Silver staining of proteins recovered after in vitro captures with 5'UTR bait (**C**) and 3'UTR bait (**D**). Aliquots of the input, supernatant and eluates of the respective coupled and empty beads were separated on a 12% SDS-Page and subjected to silver staining. **(E, F)** Volcano plots of proteins identified by in vitro capture with the 5'UTR bait (**E**) or 3'UTR bait (**F**). Significantly enriched proteins (log_2 fold change ≥ 1, p-value < 0.05) are indicated by the red dots

Next, we compared the significantly enriched proteins from the in vitro pulldowns to the proteins with a positive fold change from the in vivo large-scale capture with the *AtGRP7* 5'UTR_1 LNA oligo (without subsequent LNA2.T capture). 59 and 71 proteins overlapped between the in vivo *AtGRP7* LNA large-scale capture and the in vitro 5'UTR and 3'UTR capture, respectively, with 44 proteins being common to all three captures (Additional file 10).

Identification of novel regulators of AtGRP7

To identify potential novel regulators of the *AtGRP7* transcript, we focused on proteins with classical RBDs, which were found in more than one capture. The most abundant of these were proteins with an RRM, of which we identified 40 in total that were present in at least two of the capture experiments (Fig. 7). Moreover, we found several nuclear transport factors, RNA helicases and KH domain containing proteins (Fig. 7) in addition to several other protein groups related to RNA processing, such as translation factors, poly(A) binding proteins and small RNA related proteins (Additional file 11). But most strikingly, we identified five out of the six ALBA proteins (Fig. 7). ALBA proteins are highly conserved and found in all kingdoms of life [66]. Despite their strong conservation, they appear to have diverse functions. In archaea, ALBA proteins are mostly involved in genome packaging and organization [67], while in protozoa, they regulate RNA stability and translational [68]. In yeast and humans, ALBA proteins are involved in tRNA processing [69]. Arabidopsis encodes six ALBA proteins. ALBA1, ALBA2 and ALBA3 are short proteins, which almost solely consist of the ALBA domain, while ALBA4, ALBA5 and ALBA6 contain additional arginine-glycine

RRM-domain containing proteins

		in vivo (large-scale)		*in vitro*	
AGI	TAIR alias	*GRP7 5'UTR_1 LNA*	*GRP7 5'UTR_1 LNA + LNA2.T*	*5'UTR*	*3'UTR*
AT2G21660	GRP7	✓	✓	✓	✓
AT1G27090	-		✓	✓	✓
AT5G54900	RBP45A	✓	✓		✓
AT1G11650	RBP45B	✓		✓	✓
AT4G27000	RBP45C	✓	✓		
AT1G49600	RBP47A	✓		✓	
AT3G19130	RBP47B	✓		✓	
AT1G47490	RBP47C	✓		✓	✓
AT2G22090	UBA1A			✓	✓
AT3G56860	UBA2A	✓		✓	✓
AT2G41060	UBA2B			✓	✓
AT3G15010	UBA2C			✓	✓
AT1G54080	UBP1A	✓	✓		✓
AT1G17370	UBP1B	✓	✓	✓	✓
AT3G14100	UBP1C	✓	✓	✓	✓
AT2G32080	PUR-ALPHA-1	✓			✓
AT3G26420	ATRZ-1A	✓		✓	✓
AT5G59950	ALY1	✓			✓
AT5G02530	ALY2	✓	✓		
AT1G73530	ORRM6	✓			✓
AT4G10610	CID12	✓		✓	
AT4G03110	BRN1	✓			✓
AT1G03457	BRN2	✓	✓		
AT5G40490	HLP1			✓	✓
AT1G43190	PTB3	✓		✓	✓
AT1G48920	NUC1	✓	✓		
AT2G18510	EMB2444	✓		✓	✓
AT4G24270	EMB140			✓	✓
AT1G60000	CP28A			✓	✓
AT1G01080	CP28B	✓	✓	✓	✓
AT3G53460	CP29A			✓	✓
AT2G37220	CP29B			✓	✓
AT4G24770	CP31A	✓		✓	✓
AT5G50250	CP31B			✓	✓
AT3G52380	CP33A	✓		✓	✓
AT2G35410	CP33B	✓		✓	✓
AT4G09040	CP33C	✓		✓	✓
AT3G07810	-	✓		✓	✓
AT3G52660	-	✓		✓	✓
AT3G21215	-	✓		✓	
AT4G35785	-			✓	✓

ALBA proteins

		in vivo (large-scale)		*in vitro*	
AGI	TAIR alias	*GRP7 5'UTR_1 LNA*	*GRP7 5'UTR_1 LNA + LNA2.T*	*5'UTR*	*3'UTR*
AT1G29250	ALBA1			✓	✓
AT2G34160	ALBA2			✓	✓
AT1G76010	ALBA4	✓	✓	✓	✓
AT1G20220	ALBA5	✓	✓	✓	✓
AT3G07030	ALBA6			✓	✓

Nuclear Transport Factors

		in vivo (large-scale)		*in vitro*	
AGI	TAIR alias	*GRP7 5'UTR_1 LNA*	*GRP7 5'UTR_1 LNA + LNA2.T*	*5'UTR*	*3'UTR*
AT5G60980	ATG3BP-1	✓	✓	✓	✓
AT3G25150	ATG3BP-3	✓	✓	✓	✓
AT1G69250	ATG3BP-4	✓			✓
AT1G13730	ATG3BP-5	✓		✓	
AT2G03640	ATG3BP-6	✓			✓

Helicases

		in vivo (large-scale)		*in vitro*	
AGI	TAIR alias	*GRP7 5'UTR_1 LNA*	*GRP7 5'UTR_1 LNA + LNA2.T*	*5'UTR*	*3'UTR*
AT5G26742	RH3	✓	✓		✓
AT3G13920	RH4	✓	✓		
AT1G12770	ISE1	✓			✓
AT1G70070	ISE2	✓		✓	✓
AT5G47010	UPF1			✓	✓
AT2G03270	-			✓	✓

KH domain proteins

		in vivo (large-scale)		*in vitro*	
AGI	TAIR alias	*GRP7 5'UTR_1 LNA*	*GRP7 5'UTR_1 LNA + LNA2.T*	*5'UTR*	*3'UTR*
AT3G16230	ATKH15	✓		✓	✓
AT5G04430	ATKH22	✓	✓	✓	✓
AT3G03710	ATKH10	✓		✓	
AT4G26000	PEP			✓	✓

Fig. 7 Overview of prominent protein groups identified by in vivo and in vitro pulldowns of *AtGRP7* interactors

(RGG) repeats at their C-termini, which mediate nucleic-acid binding and protein-protein interactions [70]. ALBA1 and ALBA2 were reported to be localized in both the nucleus and the cytoplasm. In the nucleus, they bind to genic R-loops to maintain genome stability [71]. ALBA4-6 are functionally redundant, as only *alba456* triple mutants, but not single or double mutants, show pleiotropic developmental defects [52, 72]. Under heat stress, ALBA4-6 were shown to bind to selected transcripts and recruit them into phase separated stress granules and processing bodies for protection [72].

Recently, the direct in vivo target transcripts of ALBA4 were determined on a global scale via iCLIP using ALBA4-GFP lines in an *alba456* background that

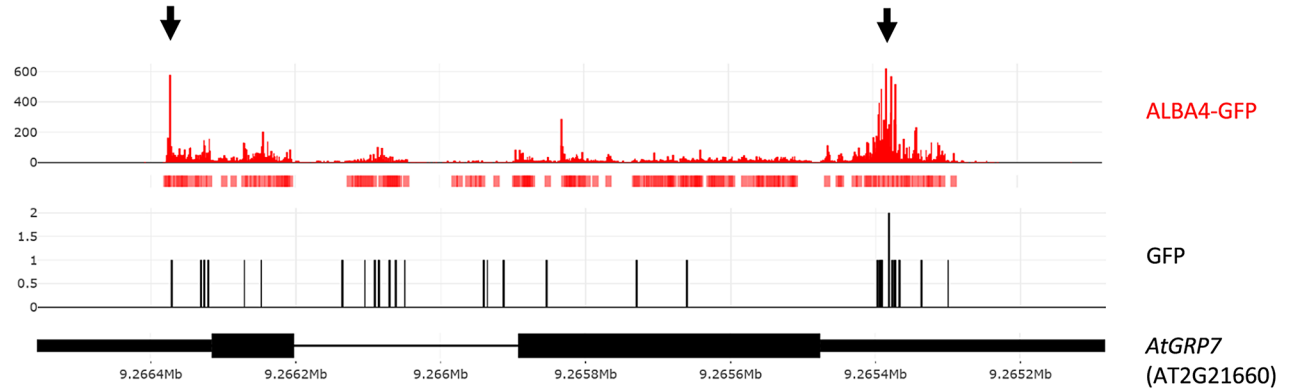

Fig. 8 In vivo binding of ALBA4 to the *AtGRP7* transcript. Binding sites of *ALBA4*::ALBA4-GFP in *alba456* to *AtGRP7* determined by iCLIP [73]. iCLIP peaks of ALBA4 are shown in red and peaks of a GFP control sample are shown in black. The red boxes below the ALBA4-GFP iCLIP reads denote called peaks. Prominent ALBA4 peaks are highlighted by arrows. The *AtGRP7* gene model is shown at the bottom. Black boxes: exons; narrow black boxes: untranslated regions; line: intron

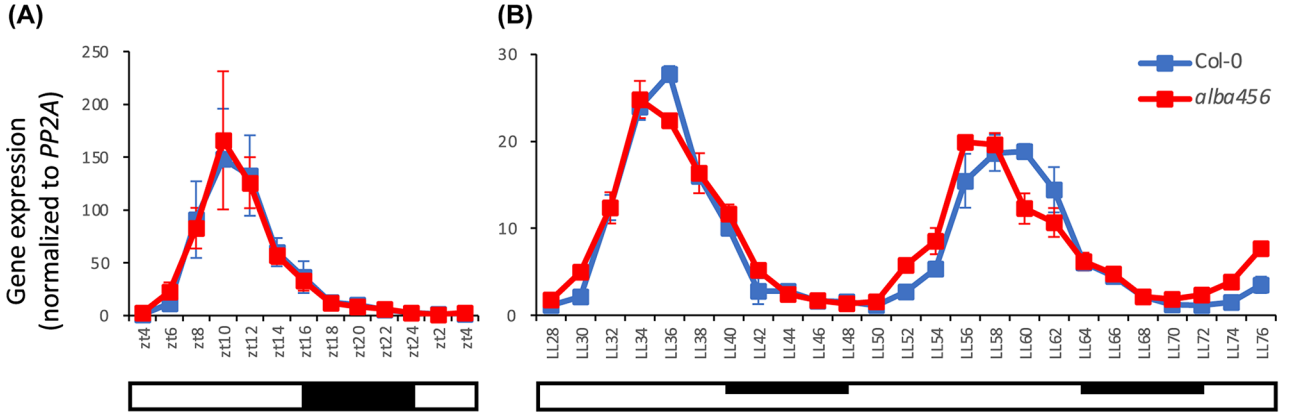

Fig. 9 Impact of altered ALBA protein levels on *AtGRP7* transcript oscillations. Col-0 wild type plants and the *alba456* triple mutant were grown in long day conditions (16 h light/8 h dark) for 12 days before transfer to constant light (LL). Seedlings were harvested at 2-h intervals throughout the light-dark cycle (**A**) and from 28 h to 76 h in LL (**B**). *AtGRP7* transcript levels were analyzed by RT-qPCR and normalized to *PP2A*. Error bars represent the standard deviation of two biological replicates. Open bar: constant light; dark bar: (subjective) night

will be reported elsewhere [73]. Plants expressing GFP under the 35S promoter were used as control. Analyzing this dataset regarding the interaction between ALBA4 and *AtGRP7*, we found many binding sites in both the *AtGRP7* 5'- and especially the 3'UTR (Fig. 8), independently validating our MS data.

To test for a functional relevance of ALBA4 binding to the *AtGRP7* transcript, we performed an extensive time course analysis in the *alba456* mutant compared to Col-0 wild type plants. Seedlings were grown in entraining long day (LD) conditions, shifted to continuous light (LL) and harvested at 2 h intervals, starting at LL28. *AtGRP7* oscillates in wild type plants with a peak at the end of the daily light period, and the oscillations persist in LL. In LD conditions, there is no difference in oscillation between Col-0 and *alba456* (Fig. 9A). In LL conditions however, *AtGRP7* levels reach the maximum about 2 h earlier in *alba456* than in Col-0, which becomes most apparent on day three in LL (Fig. 9B). Moreover, *AtGRP7* levels rise and decline faster in *alba456* than in Col-0. Even though the changes are subtle, this indicates that ALBA proteins influence the oscillation of the *AtGRP7* transcript in extended light conditions.

Discussion

Identification of the protein binding partners of a single mRNA is vital for understanding how its mRNA is regulated. So far, most studies have focused on abundant non-coding RNAs or viral RNAs and were performed in mammalian cell cultures [28, 30, 32, 36, 74, 75]. More recently, identification of proteins that bind to a germline specific transcript in *Caenorhabditis elegans* has been reported [76]. Here, we have for the first time determined the protein-binding repertoire of a single plant mRNA in vivo, using the clock regulated *AtGRP7* transcript as proof-of-concept. Towards this end, we combined and optimized elements of different RIC protocols.

Several aspects have proven critical for the success of the approach: firstly, the design of antisense oligonucleotides is key for efficient recovery of target mRNAs. We recommend testing multiple probes that bind to different regions in the transcript to optimize specificity and efficacy. In parallel to optimizing the pulldown for LNA oligonucleotides, we also compared a combination of ten antisense DNA oligonucleotides, as used in ChIRP for non-coding RNAs that were tiled across the entire *AtGRP7* transcript (sequences listed in Additional file 12). Notably, LNA antisense oligonucleotides outperformed tiled DNA oligonucleotides that were not able to enrich for the *AtGRP7* transcript in our conditions (Additional file 12) (Additional file 2, Fig. S7: Uncropped gel to Additional file 12). This could be due to coverage by translating ribosomes.

Secondly, an optimal UV crosslinking dosage is important to maximize recovery of binding proteins. For 14-day-old seedlings, we chose a dosage of 2000 mJ/cm^2, which has proven optimal in protein centric CLIP methods [18]. We have previously shown that UV stress responsive transcripts were not elevated on the fast time scale of UV crosslinking [43]. Although posttranslational modification e.g. through UV activated kinases still may impact RNA-binding properties of RBPs, any modification occurring after the formation of the covalent bond does not influence the spectrum of interactors. We recommend testing different crosslinking energies for any tissue used. At the same time, it is important to assess RNA integrity in the crosslinked sample as over-exposure can lead to RNA degradation and hence decreased mRNA recovery. The inefficient UV crosslinking, which is even more pronounced in plants due to the presence of UV-absorbing pigments like chlorophyll, combined with a limited capture efficacy of about 60% of the input makes the retrieval of specific protein interactors challenging.

Thirdly, stringent controls are necessary to discriminate specific binders from background, when working with whole plants which increases tissue complexity and unspecific binders. We opted for the mutant *grp7-1* lacking the transcript of interest, which controls for background inherent to the experimental setup. Alternatively, one could use a non-crosslinked sample or perform a pull down with scrambled oligonucleotides.

Even though we could improve the protocol for use in plants by optimizing lysis and washing buffers, shearing genomic DNA, performing two rounds of capture and considerable up-scaling to 100 g of starting material, we still detected only a small number of proteins that were significantly enriched.

Recently, a tandem RNA isolation procedure (TRIP) involving mRNA isolation followed by capture with 3'-biotinylated 2'-O-methylated RNA AOs was used to capture mRNA-protein complexes from yeast, *C. elegans* and HEK293 cells [65]. When we applied a tandem capture approach using the specific GRP7 5'UTR_1 LNA oligo first, followed by capture with LNA2.T oligonucleotides, it resulted in specific recovery of the *AtGRP7* mRNA and removal of background binders, although the number of identified proteins was small. Omitting the LNA2.T capture increased the number of identified proteins considerably, but at the cost of also capturing more unspecific binders. Nevertheless, MF GO terms for both large scale captures were linked to RNA-related terms, most notably (m)RNA binding and nucleic acid binding. Similarly, the top 10 enriched BP GO terms were connected to RNA, highlighting the value of the optimized protocol to recover interactors with a potential role in RNA regulation.

The 356 proteins identified in the large captures with two rounds of 5'UTR_1 LNA oligo were benchmarked against proteins recovered by an in vitro pulldown of nucleoplasmic proteins with either the *AtGRP7* 3'UTR or 5'UTR as a bait (Additional file 10). 59 of the in vivo identified proteins overlapped with proteins binding to the 5'UTR in vitro, and 71 overlapped with proteins binding to the 3'UTR in vitro, providing evidence for binding to the *AtGRP7* transcript. Amongst the common proteins between the in vivo and in vitro approaches were the ALBA protein family. The *AtGRP7* transcript was independently verified as target of ALBA4 by a recent iCLIP experiment, which determined strong ALBA4 binding sites in the *AtGRP7* 5'UTR and especially in the 3'UTR (Reichel et al., manuscript in preparation). By performing an extensive time course experiment, we showed that the *AtGRP7* transcript reaches its expression peak earlier in the *alba456* mutant compared to Col-0 in extended light conditions, suggesting that ALBA proteins alter the oscillation of *AtGRP7*. Although the observed effect is rather mild under standard growth conditions, it is possible that there is a more pronounced effect under stress, since both *At*GRP7 and ALBA proteins are involved in stress response [72, 77, 78].

Conclusion

We adapted specific RNA interactome capture for use in plants, using *AtGRP7* as a showcase, and identified the ALBA4 protein as a new regulator. Since *AtGRP7* is one of the most abundant mRNAs at its expression peak, the protocol will still need optimization and up-scaling to be applicable for other less abundant mRNAs and to cover the whole spectrum of interacting proteins. To increase the yield of recovered proteins, this protocol could be used with a more potent crosslinking reagent, like formaldehyde, instead of UV light. However, this would have the disadvantage of recovering both direct and indirect interactors. Continuous improvements of

mass spectrometry sensitivity will also help to increase the range of identified proteins.

Abbreviations

ALBA	Acetylation Lowers Binding Affinity
AO	antisense oligonucleotide
ASCO	Alternative Splicing Competitor
AtGRP7	Arabidopsis thaliana GLYCINE RICH RNA-BINDING PROTEIN 7
BAP	beads after pulldown
BBP	beads before pulldown
CHART	Capture Hybridization Analysis of RNA Targets
EDC-HCl	*N*-(3-dimethylaminopropyl)-*N'*-ethylcarbodiimide hydrochloride
eRIC	enhanced RNA interactome capture
gDNA	genomic DNA
GFP	Green fluorescent protein
GO	Gene ontology
h	hour
HCD	Higher-energy collisional dissociation
iCLIP	individual-nucleotide resolution crosslinking and immunoprecipitation
IN	input
LD	light-dark
LL	continuous light
LNA	locked nucleic acid
lncRNA	long noncoding RNA
MALAT1	metastasis-associated lung adenocarcinoma transcript 1
MES	2-(N-morpholino)ethanesulfonic acid
min	minute
MS	Mass spectrometry
NEAT1	nuclear-enriched abundant transcript 1
NSRa	Nuclear Speckle Rna-Binding Protein a
PBS	phosphate buffered saline
PCR	Polymerase chain reaction
PHAROH	Pluripotency and Hepatocyte Associated RNA Overexpressed in HCC
PVP40	polyvinylpyrrolidone 40
PWB	protein wash buffer
RBPome	RNA binding proteome
RIC	RNA interactome capture
RNP	Ribonucleoprotein
RT	reverse transcription
SN	supernatant
snRNA	small nuclear RNA
SSC	saline sodium citrate
UTR	untranslated region
UV	light ultraviolet light

Supplementary Information

The online version contains supplementary material available at https://doi.org/10.1186/s12870-024-05249-4.

Supplementary Material 1

Supplementary Material 2

Supplementary Material 3

Supplementary Material 4

Supplementary Material 5

Supplementary Material 6

Supplementary Material 7

Supplementary Material 8

Supplementary Material 9

Supplementary Material 10

Supplementary Material 11

Supplementary Material 12

Acknowledgements

We thank Elisabeth Klemme and Kristina Neudorf for expert technical assistance and Anthony Millar and Naiqi Wang (ANU, Canberra) for providing the ALBA4-GFP and 35 S-GFP lines. We thank Dr. Zhicheng Zhang for valuable comments on the manuscript. Figures were created with Biorender.

Author contributions

D.S. and M. Reichel performed project conception and design. M. Reichel performed in vivo pulldowns. O.S. performed in vitro pulldowns. M. Rettel and F.S. performed proteomics analysis of the in vivo pulldowns and 5´UTR in vitro pulldowns. F.B. performed proteomics analysis of the 3´UTR in vitro pulldowns. T.K. provided advice on pulldowns. M. Reichel and D.S. wrote the main manuscript text. M. Reichel prepared the figures. All authors reviewed the manuscript.

Funding

The project was supported by the German Research Foundation (DFG) through grant STA653/13 and a postdoctoral fellowship of the Alexander von Humboldt Foundation to MR.
Open Access funding enabled and organized by Projekt DEAL.

Data availability

The mass spectrometry proteomics data have been deposited to the ProteomeXchange Consorti-um via the PRIDE [79] partner repository with the dataset identifiers PXD048975 and PXD049303.

Ethics approval and consent to participate

Not applicable.

Consent for publication

Not applicable.

Competing interests

The authors declare no competing interests.

Received: 14 March 2024 / Accepted: 5 June 2024
Published online: 14 June 2024

References

1. Singh G, Pratt G, Yeo GW, Moore MJ. The clothes make the mRNA: past and Present trends in mRNP Fashion. Annu Rev Biochem. 2015;84(1):325–54.
2. Glisovic T, Bachorik JL, Yong J, Dreyfuss G. RNA-binding proteins and post-transcriptional gene regulation. FEBS Lett. 2008;582(14):1977–86.
3. Mateos JL, Staiger D. Toward a systems view on RNA-binding proteins and associated RNAs in plants: guilt by association. Plant Cell. 2023;35(6):1708–26.
4. Castello A, Fischer B, Eichelbaum K, Horos R, Beckmann B, Strein C, Davey Norman E, Humphreys David T, Preiss T, Steinmetz L, et al. Insights into RNA Biology from an Atlas of mammalian mRNA-Binding proteins. Cell. 2012;149(6):1393–406.
5. Baltz AG, Munschauer M, Schwanhäusser B, Vasile A, Murakawa Y, Schueler M, Youngs N, Penfold-Brown D, Drew K, Milek M, et al. The mRNA-Bound proteome and its global occupancy Profile on protein-coding transcripts. Mol Cell. 2012;46(5):674–90.
6. Matia-Gonzalez AM, Laing EE, Gerber AP. Conserved mRNA-binding proteomes in eukaryotic organisms. Nat Struct Mol Biol. 2015;22(12):1027–33.
7. Mitchell SF, Jain S, She M, Parker R. Global analysis of yeast mRNPs. Nat Struct Mol Biol. 2013;20(1):127–33.
8. Beckmann BM, Horos R, Fischer B, Castello A, Eichelbaum K, Alleaume A-M, Schwarzl T, Curk T, Foehr S, Huber W, et al. The RNA-binding proteomes from yeast to man harbour conserved enigmRBPs. Nat Commun. 2015;6:10127.
9. Sysoev VO, Fischer B, Frese CK, Gupta I, Krijgsveld J, Hentze MW, Castello A, Ephrussi A. Global changes of the RNA-bound proteome during the maternal-to-zygotic transition in Drosophila. Nat Commun. 2016;7:12128.
10. Wessels H-H, Imami K, Baltz AG, Kolinski M, Beldovskaya A, Selbach M, Small S, Ohler U, Landthaler M. The mRNA-bound proteome of the early fly embryo. Genome Res. 2016;26(7):1000–9.
11. Hentze MW, Castello A, Schwarzl T, Preiss T. A brave new world of RNA-binding proteins. Nat Rev Mol Cell Biol. 2018;19(5):327–41.

12. Wahlestedt C, Salmi P, Good L, Kela J, Johnsson T, Hökfelt T, Broberger C, Porreca F, Lai J, Ren K, et al. Potent and nontoxic antisense oligonucleotides containing locked nucleic acids. Proc Natl Acad Sci USA. 2000;97(10):5633–8.
13. Marondedze C, Thomas L, Serrano NL, Lilley KS, Gehring C. The RNA-binding protein repertoire of Arabidopsis thaliana. Sci Rep. 2016;6:29766.
14. Zhang Z, Boonen K, Ferrari P, Schoofs L, Janssens E, van Noort V, Rolland F, Geuten K. UV crosslinked mRNA-binding proteins captured from leaf mesophyll protoplasts. Plant Methods. 2016;12(1):42.
15. Reichel M, Liao Y, Rettel M, Ragan C, Evers M, Alleaume A-M, Horos R, Hentze MW, Preiss T, Millar AA. In planta determination of the mRNA-binding proteome of Arabidopsis etiolated seedlings. Plant Cell. 2016;28:2435–52.
16. Köster T, Marondedze C, Meyer K, Staiger D. RNA-binding proteins revisited – the emerging Arabidopsis mRNA interactome. Trends Plant Sci. 2017;22(6):512–26.
17. Van Ende R, Balzarini S, Geuten K. Single and combined methods to specifically or bulk-purify RNA–Protein complexes. Biomolecules. 2020;10(8):1160.
18. Köster T, Reichel M, Staiger D. CLIP and RNA interactome studies to unravel genome-wide RNA-protein interactions in vivo in Arabidopsis thaliana. Methods. 2020;178:63–71.
19. Liu L, Trendel J, Jiang G, Liu Y, Bruckmann A, Küster B, Sprunck S, Dresselhaus T, Bleckmann A. RBPome identification in egg-cell like callus of Arabidopsis. Biol Chem. 2023;(11–12):1137–49.
20. Bach-Pages M, Homma F, Kourelis J, Kaschani F, Mohammed S, Kaiser M, van der Hoorn RAL, Castello A, Preston GM. Discovering the RNA-Binding proteome of Plant leaves with an improved RNA interactome capture Method. Biomolecules. 2020;10(4):661.
21. Grabowski PJ, Sharp PA. Affinity chromatography of splicing complexes: U2, U5, and U4 + U6 small nuclear ribonucleoprotein particles in the spliceosome. Science. 1986;233(4770):1294–9.
22. Johansson HE, Liljas L, Uhlenbeck OC. RNA recognition by the MS2 phage coat protein. Seminars Virol. 1997;8(3):176–85.
23. Said N, Rieder R, Hurwitz R, Deckert J, Urlaub H, Vogel J. In vivo expression and purification of aptamer-tagged small RNA regulators. Nucleic Acids Res. 2009;37(20):e133.
24. Lüders J, Winkel AR, Reichel M, Bitterer VW, Scheibe M, Widmann C, Butter F, Köster T. Identification of Pri-miRNA Stem-Loop interacting proteins in plants using a Modified Version of the Csy4 CRISPR Endonuclease. Int J Mol Sci. 2022;23(16):8961.
25. Lee HY, Haurwitz RE, Apffel A, Zhou K, Smart B, Wenger CD, Laderman S, Bruhn L, Doudna JA. RNA–protein analysis using a conditional CRISPR nuclease. Proc Natl Acad Sci USA. 2013;110(14):5416–21.
26. Hutchinson JN, Ensminger AW, Clemson CM, Lynch CR, Lawrence JB, Chess A. A screen for nuclear transcripts identifies two linked noncoding RNAs associated with SC35 splicing domains. BMC Genomics. 2007;8:39.
27. Ulitsky I, Shkumatava A, Jan CH, Sive H, Bartel DP. Conserved function of lincRNAs in vertebrate embryonic development despite rapid sequence evolution. Cell. 2011;147(7):1537–50.
28. West Jason A, Davis Christopher P, Sunwoo H, Simon Matthew D, Sadreyev Ruslan I, Wang Peggy I, Tolstorukov Michael Y. Kingston Robert E: the long noncoding RNAs NEAT1 and MALAT1 bind active chromatin sites. Mol Cell. 2014;55(5):791–802.
29. Simon MD, Wang CI, Kharchenko PV, West JA, Chapman BA, Alekseyenko AA, Borowsky ML, Kuroda MI, Kingston RE. The genomic binding sites of a noncoding RNA. Proc Natl Acad Sci USA. 2011;108(51):20497–502.
30. Chu C, Zhang Qiangfeng C, da Rocha Simão T, Flynn Ryan A, Bharadwaj M, Calabrese JM, Magnuson T, Heard E, Chang Howard Y. Systematic Discovery of Xist RNA binding proteins. Cell. 2015;161(2):404–16.
31. Mangilet AF, Weber J, Schüler S, Droste-Borel I, Streicher S, Schmutzer T, Rot G, Macek B, Laubinger S. The Arabidopsis U1 snRNP regulates mRNA 3'-end processing. *bioRxiv* 2023:2023.2009.2019.558503.
32. McHugh CA, Chen C-K, Chow A, Surka CF, Tran C, McDonel P, Pandya-Jones A, Blanco M, Burghard C, Moradian A, et al. The Xist lncRNA interacts directly with SHARP to silence transcription through HDAC3. Nature. 2015;521(7551):232–6.
33. Yu AT, Berasain C, Bhatia S, Rivera K, Liu B, Rigo F, Pappin DJ, Spector DL. PHAROH lncRNA regulates Myc translation in hepatocellular carcinoma via sequestering TIAR. eLife. 2021;10:e68263.
34. Bardou F, Ariel F, Simpson Craig G, Romero-Barrios N, Laporte P, Balzergue S, Brown John WS, Crespi M. Long noncoding RNA modulates alternative splicing regulators in Arabidopsis. Dev Cell. 2014;30(2):166–76.
35. Rigo R, Bazin J, Romero-Barrios N, Moison M, Lucero L, Christ A, Benhamed M, Blein T, Huguet S, Charon C, et al. The Arabidopsis lncRNA ASCO modulates the transcriptome through interaction with splicing factors. EMBO Rep. 2020;21(5):e48977.
36. Rogell BM, Fischer B, Rettel M, Krijgsveld J, Castello A, Hentze MW. Specific RNP capture with antisense LNA/DNA mixmers. RNA. 2017;23(8):1290–302.
37. Heintzen C, Melzer S, Fischer R, Kappeler S, Apel K, Staiger D. A light- and temperature-entrained circadian clock controls expression of transcripts encoding nuclear proteins with homology to RNA-binding proteins in meristematic tissue. Plant J. 1994;5(6):799–813.
38. Carpenter CD, Kreps JA, Simon AE. Genes encoding glycine-rich *Arabidopsis thaliana* proteins with RNA-binding motifs are influenced by cold treatment and an endogenous circadian rhythm. Plant Physiol. 1994;104(3):1015–25.
39. Heintzen C, Nater M, Apel K, Staiger D. *At*GRP7, a nuclear RNA-binding protein as a component of a circadian-regulated negative feedback loop in *Arabidopsis thaliana*. Proc Natl Acad Sci USA. 1997;94:8515–20.
40. Schöning JC, Streitner C, Page DR, Hennig S, Uchida K, Wolf E, Furuya M, Staiger D. Autoregulation of the circadian slave oscillator component *At*GRP7 and regulation of its targets is impaired by a single RNA recognition motif point mutation. Plant J. 2007;52:1119–30.
41. Schöning JC, Streitner C, Meyer IM, Gao Y, Staiger D. Reciprocal regulation of glycine-rich RNA-binding proteins via an interlocked feedback loop coupling alternative splicing to nonsense-mediated decay in Arabidopsis. Nucleic Acids Res. 2008;36:6977–87.
42. Staiger D, Zecca L, Wieczorek Kirk DA, Apel K, Eckstein L. The circadian clock regulated RNA-binding protein AtGRP7 autoregulates its expression by influencing alternative splicing of its own pre-mRNA. Plant J. 2003;33(2):361–71.
43. Meyer K, Köster T, Nolte C, Weinholdt C, Lewinski M, Grosse I, Staiger D. Adaptation of iCLIP to plants determines the binding landscape of the clock-regulated RNA-binding protein AtGRP7. Genome Biol. 2017;18(1):204.
44. Staiger D, Apel K. Circadian clock-regulated expression of an RNA-binding protein in Arabidopsis: characterisation of a minimal promoter element. Mol Gen Genet. 1999;261(4–5):811–9.
45. Schmal C, Reimann P, Staiger D. A circadian clock-regulated toggle switch explains AtGRP7 and AtGRP8 oscillations in Arabidopsis thaliana. PLoS Comput Biol. 2013;9(3):e1002986.
46. Fu ZQ, Guo M, Jeong BR, Tian F, Elthon TE, Cerny RL, Staiger D, Alfano JR. A type III effector ADP-ribosylates RNA-binding proteins and quells plant immunity. Nature. 2007;447(7142):284–8.
47. Streitner C, Danisman S, Wehrle F, Schöning JC, Alfano JR, Staiger D. The small glycine-rich RNA-binding protein *At*GRP7 promotes floral transition in *Arabidopsis thaliana*. Plant J. 2008;56:239–50.
48. Steffen A, Elgner M, Staiger D. Regulation of Flowering Time by the RNA-Binding proteins AtGRP7 and AtGRP8. Plant Cell Physiol. 2019;60(9):2040–50.
49. Lewinski M, Steffen A, Kachariya N, Elgner M, Schmal C, Messini N, Koster T, Reichel M, Sattler M, Zarnack K, et al. Arabidopsis thaliana GLYCINE RICH RNA-BINDING PROTEIN 7 interaction with its iCLIP target LHCB1.1 correlates with changes in RNA stability and circadian oscillation. Plant J. 2024;118(1):203–24.
50. Streitner C, Köster T, Simpson CG, Shaw P, Danisman S, Brown JWS, Staiger D. An hnRNP-like RNA-binding protein affects alternative splicing by in vivo interaction with target transcripts in Arabidopsis thaliana. Nucleic Acids Res. 2012;40(22):11240–55.
51. Köster T, Meyer K, Weinholdt C, Smith LM, Lummer M, Speth C, Grosse I, Weigel D, Staiger D. Regulation of pri-miRNA processing by the hnRNP-like protein AtGRP7 in Arabidopsis. Nucleic Acids Res. 2014;42(15):9925–36.
52. Wang N, Jalajakumari M, Miller T, Asadi M, Millar AA. The ALBA RNA-binding proteins function redundantly to promote growth and flowering in Arabidopsis. bioRxiv 2019:758946.
53. Murashige T, Skoog F. A revised medium for rapid growth and bio assays with tobacco tissue cultures. Physiol Plant. 1962;15:473–97.
54. Lewinski M, Brüggemann M, Köster T, Reichel M, Bergelt T, Meyer K, König J, Zarnack K, Staiger D. Mapping protein–RNA binding in plants with individual-nucleotide-resolution UV cross-linking and immunoprecipitation (plant iCLIP2). Nat Protoc 2024.
55. Perez-Perri JI, Rogell B, Schwarzl T, Stein F, Zhou Y, Rettel M, Brosig A, Hentze MW. Discovery of RNA-binding proteins and characterization of their dynamic responses by enhanced RNA interactome capture. Nat Commun. 2018;9(1):4408.
56. Hughes CS, Foehr S, Garfield DA, Furlong EE, Steinmetz LM, Krijgsveld J. Ultrasensitive proteome analysis using paramagnetic bead technology. Mol Syst Biol. 2014;10(10):757.
57. Hughes CS, Moggridge S, Müller T, Sorensen PH, Morin GB, Krijgsveld J. Single-pot, solid-phase-enhanced sample preparation for proteomics experiments. Nat Protoc. 2019;14(1):68–85.

58. Dayon L, Hainard A, Licker V, Turck N, Kuhn K, Hochstrasser DF, Burkhard PR, Sanchez J-C. Relative quantification of proteins in human cerebrospinal fluids by MS/MS using 6-Plex isobaric tags. Anal Chem. 2008;80(8):2921–31.
59. Franken H, Mathieson T, Childs D, Sweetman GMA, Werner T, Tögel I, Doce C, Gade S, Bantscheff M, Drewes G, et al. Thermal proteome profiling for unbiased identification of direct and indirect drug targets using multiplexed quantitative mass spectrometry. Nat Protoc. 2015;10(10):1567–93.
60. Team RDC. R: a language and environment for statistical computing. R Foundation for Statistical Computing; 2009.
61. Huber W, von Heydebreck A, Sültmann H, Poustka A, Vingron M. Variance stabilization applied to microarray data calibration and to the quantification of differential expression. Bioinformatics. 2002;18(suppl1):S96–104.
62. Ritchie ME, Phipson B, Wu D, Hu Y, Law CW, Shi W, Smyth GK. Limma powers differential expression analyses for RNA-sequencing and microarray studies. Nucleic Acids Res. 2015;43(7):e47.
63. Staiger D, Kaulen H, Schell J. A CACGTG motif of the Antirrhinum majus chalcone synthase promoter is recognized by an evolutionarily conserved nuclear protein. Proc Natl Acad Sci USA. 1989;86(18):6930–4.
64. Hafner M, Katsantoni M, Köster T, Marks J, Mukherjee J, Staiger D, Ule J, Zavolan M. CLIP and complementary methods. Nat Reviews Methods Primers. 2021;1(1):20.
65. Matia-González AM, Iadevaia V, Gerber AP. A versatile tandem RNA isolation procedure to capture in vivo formed mRNA-protein complexes. Methods. 2017;118–119:93–100.
66. Verma JK, Gayali S, Dass S, Kumar A, Parveen S, Chakraborty S, Chakraborty N. OsAlba1, a dehydration-responsive nuclear protein of rice (Oryza sativa L. ssp. indica), participates in stress adaptation. Phytochemistry. 2014;100:16–25.
67. Laurens N, Driessen RPC, Heller I, Vorselen D, Noom MC, Hol FJH, White MF, Dame RT, Wuite GJL. Alba shapes the archaeal genome using a delicate balance of bridging and stiffening the DNA. Nat Commun. 2012;3(1):1328.
68. Mani J, Güttinger A, Schimanski B, Heller M, Acosta-Serrano A, Pescher P, Späth G, Roditi I. Alba-Domain proteins of Trypanosoma Brucei are cytoplasmic RNA-Binding proteins that interact with the translation Machinery. PLoS ONE. 2011;6(7):e22463.
69. Aravind L, Iyer LM, Anantharaman V. The two faces of Alba: the evolutionary connection between proteins participating in chromatin structure and RNA metabolism. Genome Biol. 2003;4(10):R64.
70. Thandapani P, O'Connor TR, Bailey TL, Richard S. Defining the RGG/RG motif. Mol Cell. 2013;50(5):613–23.
71. Yuan W, Zhou J, Tong J, Zhuo W, Wang L, Li Y, Sun Q, Qian W. ALBA protein complex reads genic R-loops to maintain genome stability in Arabidopsis. Sci Adv. 2019;5(5):eaav9040.
72. Tong J, Ren Z, Sun L, Zhou S, Yuan W, Hui Y, Ci D, Wang W, Fan L-M, Wu Z, et al. ALBA proteins confer thermotolerance through stabilizing HSF messenger RNAs in cytoplasmic granules. Nat Plants. 2022;8(7):778–91.
73. Reichel M, Due Tankmar M, Rennie S, Arribaz-Hernandez L, Lewinski M, Köster T, Wang B, Millar AA, Staiger D, Brodersen P. ALBA proteins facilitate cytoplasmic YTHDF-mediated reading of m6A in plants. BioRxiv. 2024. https://doi.org/10.1101/2024.06.06.597704
74. Minajigi A, Froberg JE, Wei C, Sunwoo H, Kesner B, Colognori D, Lessing D, Payer B, Boukhali M, Haas W, et al. A comprehensive Xist interactome reveals cohesin repulsion and an RNA-directed chromosome conformation. Science. 2015;349(6245):aab2276.
75. Phillips SL, Garcia-Blanco MA, Bradrick SS. Antisense-mediated affinity purification of dengue virus ribonucleoprotein complexes from infected cells. Methods. 2015;91:13–9.
76. Theil K, Imami K, Rajewsky N. Identification of proteins and miRNAs that specifically bind an mRNA in vivo. Nat Commun. 2019;10(1):4205.
77. Cao S, Jiang L, Song S, Jing R, Xu G. AtGRP7 is involved in the regulation of abscisic acid and stress responses in *Arabidopsis*. Cell Mol Biol Lett. 2006;11:526–35.
78. Kim JS, Park SJ, Kwak KJ, Kim YO, Kim JY, Song J, Jang B, Jung CH, Kang H. Cold shock domain proteins and glycine-rich RNA-binding proteins from Arabidopsis thaliana can promote the cold adaptation process in Escherichia coli. Nucleic Acids Res. 2007;35:506–16.
79. Perez-Riverol Y, Bai J, Bandla C, García-Seisdedos D, Hewapathirana S, Kamatchinathan S, Kundu Deepti J, Prakash A, Frericks-Zipper A, Eisenacher M, et al. The PRIDE database resources in 2022: a hub for mass spectrometry-based proteomics evidences. Nucleic Acids Res. 2021;50(D1):D543–52.

Publisher's Note